

長崎大学

宮崎泰司 業績リスト

| 発表者名 | 論文タイトル名 | 発表誌名 | 巻号 | ページ | 出版年 |
|--|---|-------------------|-----|---------|------|
| Masamitsu Yanada, Jin Takeuchi, Isamu Sugiura, Hideki Akiyama, Noriko Usui, Fumiharu Yagasaki, Kazuhiro Nishii, Yasunori Ueda, Makoto Takeuchi, Shuichi Miyawaki, Atsuo Maruta, Hiroto Narimatsu, Yasushi Miyazaki, Shigeki Ohtake, Itsuro Jinnai, Keitaro Matsuo, Tomoki Naoe, and Ryuzo Ohno, for the Japan Adult Leukemia Study Group | Karyotype at diagnosis is the major prognostic factor predicting relapse-free survival for patients with Philadelphia chromosome-positive acute lymphoblastic leukemia treated with imatinib-combined chemotherapy. | Haematologica. | 93 | 287-290 | 2008 |
| Akira Matsuda, Itsuro Jinnai, Yasushi Miyazaki, Masao Tomonaga | Proposals for a grading system for diagnostic accuracy of the Myelodysplastic syndromes. | Clinical Leukemia | 2 | 102-106 | 2008 |
| Yasushi Sawayama, Yasushi Miyazaki, Koji Ando, Kensuke Horio, Chizuko Tsutsumi, Daisuke Imanishi, Hideki Tsushima, Yoshitaka Imaizumi, Tomoko Hata, Takuya Fukushima, Shinichiro Yoshida, Yasuyuki Onimaru, Masako Iwanaga, Jun Taguchi, Kazutaka Kuriyama, Masao Tomonaga. | Expression of myeloperoxidase enhances the chemosensitivity of leukemia cells through the generation of reactive oxygen species and the nitration of protein. | Leukemia | 22 | 956-964 | 2008 |
| Wakui M, Kuriyama K, Miyazaki Y, Hata T, Taniwaki M, Ohtake S, Sakamaki H, Miyawaki S, Naoe T, Ohno R, Tomonaga M | Diagnosis of acute myeloid leukemia according to the WHO classification in the Japan Adult Leukemia Study Group AML-97 protocol. | Int J Hematol | 87 | 144-151 | 2008 |
| Suzuki T, Tomonaga M, Miyazaki Y, Nakao S, Ohyashiki K, Matsumura I, Kohgo Y, Niitsu Y, Kojima S, Ozawa K. | Japanese epidemiological survey with consensus statement on Japanese guidelines for treatment of iron overload in bone marrow failure syndromes. | Int J Hematol | 88 | 30-35 | 2008 |
| Yanada M, Sugiura I, Takeuchi J, Akiyama H, Maruta A, Ueda Y, Usui N, Yagasaki F, Yujiri T, Takeuchi M, Nishii K, Kimura Y, Miyawaki S, Narimatsu H, Miyazaki Y, Ohtake S, Jinnai I, Matsuo K, Naoe T, Ohno R. for the Japan Adult Leukemia Study Group | Prospective monitoring of BCR-ABL transcript levels in patients with Philadelphia chromosome-positive acute lymphoblastic leukaemia undergoing imatinib-combined chemotherapy.s | Brit J Haematol | 143 | 503-510 | 2008 |
| Masako Iwanaga, Masuko Tagawa, Kunihiro Tsukasaki, Tatsuki Matsuo, Ken-ichi Yokota, Yasushi Miyazaki, Takuya Fukushima, Tomoko Hata, Yoshitaka Imaizumi, Daisuke Imanishi, Jun Taguchi, Sabro Momita, Shimeru Kamihira, and Masao Tomonaga | Relationship between Monoclonal Gammopathy of Undetermined Significance and Radiation Exposure in Nagasaki Atomic Bomb Survivors. | Blood | | on line | 2008 |
| Takuya Fukushima, Kensuke Horio, Emi Matsuo, Daisuke Imanishi, Reishi Yamasaki, Hideki Tsushima, Yoshitaka Imaizumi, Koichi Ohshima, Tomoko Hata, Shinichiro Yoshida, Yasushi Miyazaki, Masao Tomonaga. | Successful cord blood transplantation for Mycosis fungoides. | Int J Hematol | 88 | 596-598 | 2008 |

| | | | | | |
|---|--|----------------------|--|-----------------|-------------|
| <p>Mari Sakai, Yasushi Miyazaki, Emi Matsuo, Yukiyoichi Moriuchi, Tomoko Hata, Takuya Fukushima, Yoshitaka Imaizumi, Daisuke Imanishi, Jun Taguchi, Masako Iwanaga, Hideki Tsushima, Yoriko Inoue, Yumi Takasaki, Takeshi Tsuchiya, Minoru Komoda, Koji Ando, Kensuke Horio, Yuji Moriwaki, Shinya Tominaga, Hidehiro Itonaga, Kazuhiro Nagai, Kunihiro Tsukasaki, Chizuko Tsutsumi, Yasushi Sawayama, Reishi Yamasaki, Daisuke Ogawa, Yasuhisa Kawaguchi, Shuichi Ikeda, Shinichiro Yoshida, Yasuyuki Onimaru, Masayuki Tawara, Sunao Atogami, Satoshi Koida, Tatsuro Joh, Masaomi Yamamura, Yuji Matsuo, Hisashi Soda, Hiroaki Nonaka, Itsuro Jinnai, Kazutaka Kuriyama, Masao Tomonaga</p> | <p>Long-term efficacy of imatinib in a practical setting is correlated with imatinib trough concentration that is influenced by body size: a report by the Nagasaki CML Study Group.</p> | <p>Int J Hematol</p> | | <p>in press</p> | <p>2009</p> |
|---|--|----------------------|--|-----------------|-------------|

A mouse model for *EML4-ALK*-positive lung cancer

Manabu Soda^{a,b}, Shuji Takada^a, Kengo Takeuchi^c, Young Lim Choi^a, Munehiro Enomoto^a, Toshihide Ueno^a, Hidenori Haruta^a, Toru Hamada^a, Yoshihiro Yamashita^a, Yuichi Ishikawa^c, Yukihiko Sugiyama^b, and Hiroyuki Mano^{a,d,1}

Divisions of ^aFunctional Genomics and ^bPulmonary Medicine, Jichi Medical University, Tochigi 329-0498, Japan; ^cDivision of Pathology, The Cancer Institute, Japanese Foundation for Cancer Research, Tokyo 135-8550, Japan; and ^dCore Research for Evolutional Science and Technology, Japan Science and Technology Agency, Saitama 332-0012, Japan

Edited by John D. Minna, University of Texas Southwestern Medical Center, Dallas, TX, and accepted by the Editorial Board October 17, 2008 (received for review June 2, 2008)

EML4-ALK is a fusion-type protein tyrosine kinase that is generated in human non-small-cell lung cancer (NSCLC) as a result of a recurrent chromosome inversion, *inv*(2)(p21p23). Although mouse 3T3 fibroblasts expressing human EML4-ALK form transformed foci in culture and s.c. tumors in nude mice, it has remained unclear whether this fusion protein plays an essential role in the carcinogenesis of NSCLC. To address this issue, we have now established transgenic mouse lines that express EML4-ALK specifically in lung alveolar epithelial cells. All of the transgenic mice examined developed hundreds of adenocarcinoma nodules in both lungs within a few weeks after birth, confirming the potent oncogenic activity of the fusion kinase. Although such tumors underwent progressive enlargement in control animals, oral administration of a small-molecule inhibitor of the kinase activity of ALK resulted in their rapid disappearance. Similarly, whereas i.v. injection of 3T3 cells expressing EML4-ALK induced lethal respiratory failure in recipient nude mice, administration of the ALK inhibitor effectively cleared the tumor burden and improved the survival of such animals. These data together reinforce the pivotal role of EML4-ALK in the pathogenesis of NSCLC in humans, and they provide experimental support for the treatment of this intractable cancer with ALK inhibitors.

transgenic mouse | surfactant protein C | molecular targeted therapy

Lung cancer remains the leading cause of cancer deaths, with almost 1.3 million people dying annually from this condition worldwide (www.who.int/cancer/en). Although a variety of chemotherapeutic regimens have been developed to treat this intractable disease, their efficacy is limited and depends on cancer subtype. Non-small-cell lung cancer (NSCLC) accounts for 80–85% of all lung cancer cases and is less sensitive to cytotoxic drugs than is small cell lung cancer. Unless tumor cells are surgically resected at an early clinical stage, individuals with NSCLC can expect a median survival time of less than 1 year (1).

A subset of individuals with NSCLC (mostly nonsmokers, young females, and those of Asian ethnicity) have been shown to harbor mutations in the epidermal growth factor receptor (EGFR) gene (2–4). Such mutations result in constitutive activation of the EGFR tyrosine kinase, the oncogenic potential of which has been demonstrated in a transgenic mouse system (5). Small-molecule drugs that specifically inhibit the catalytic activity of EGFR have been found to exhibit clinical efficacy in the treatment of NSCLC patients, especially in those with an activated EGFR (6, 7).

We recently developed a system for the construction of retroviral cDNA libraries from small quantities of clinical specimens (8–10), and we applied this technology to NSCLC to screen for oncogenes that might be potential drug targets (11). With the use of a focus-formation assay performed with mouse 3T3 fibroblasts, we identified a fusion-type oncogene, *EML4-ALK*, in an NSCLC specimen of a smoker (12). A small inversion within the short arm of chromosome 2 was found to result in the ligation of *EML4* and *ALK*, leading to the production of a fusion protein consisting of the amino-terminal portion of EML4 and the intracellular region of the protein tyrosine kinase ALK. The

coiled-coil domain within this portion of EML4 mediates the constitutive dimerization and activation of EML4-ALK, which is responsible for the generation of transformed cell foci in culture and the formation by these cells of s.c. tumors in nude mice. Although the *inv*(2)(p21p23) rearrangement responsible for the fusion event occurs recurrently in NSCLC patients, it remains to be demonstrated that *EML4-ALK* plays an essential role in the carcinogenesis of NSCLC harboring the fusion gene.

To address this issue, we have now engineered the expression of *EML4-ALK* in lung epithelial cells of transgenic mice. The surfactant protein C gene (*SPC*) is specifically expressed in type 2 alveolar epithelial cells, and a fragment of its promoter has been used widely for establishment of mouse lines that express transgenes specifically in lung epithelial cells (13–15). We therefore generated independent mouse lines in which *EML4-ALK* expression is driven by the *SPC* promoter, and we found that all such mice develop hundreds of adenocarcinoma nodules in both lungs within only a few weeks after birth. Furthermore, inhibition of EML4-ALK activity with a small-molecule drug induced rapid death of the tumor cells.

Results

Generation of *EML4-ALK* Transgenic Mice. To generate mice with lung-specific expression of *EML4-ALK*, we ligated a fragment of the *SPC* promoter (≈3.7 kbp) to a cDNA for EML4-ALK variant 1 with an amino-terminal FLAG epitope tag (12). The cDNA was, in turn, attached to an RNA splicing cassette and a polyadenylation signal (Fig. 1A). The transgene construct (≈8.3 kbp) was then injected into pronuclear-stage embryos of C57BL/6J mice, and the resulting progeny were screened for the presence of the transgene by Southern blot analysis. Seven founder mice positive for incorporation of the transgene (copy number per diploid genome ranging from 1 to 30) were obtained (Fig. 1B and data not shown). Two transgenic lines (501-3 and 502-4, with 10 and 30 copies of the transgene per genome, respectively) were independently maintained by backcrossing to C57BL/6J mice. To confirm the lung-specific expression of the transgene, we performed RT-PCR analysis to detect *EML4-ALK* mRNA in an F₁ mouse of the 502-4 line. The transgene was expressed in lung tissue (containing adenocarcinoma nodules, see below) but not in liver, esophagus, stomach, colon, brain, kidney, or uterus (Fig. 1C).

Detection of Multiple Lung Adenocarcinoma Nodules in the Transgenic Mice. One founder mouse (503-6, with 3 copies of the transgene per genome) (Fig. 1B) died 3 weeks after birth. Postmortem

Author contributions: Y.I., Y.S., and H.M. designed research; M.S., S.T., K.T., Y.L.C., M.E., T.U., H.H., T.H., Y.Y., and Y.I. performed research; and H.M. wrote the paper.

Conflict of interest statement: K.T. is a consultant for Dako.

This article is a PNAS Direct Submission. J.D.M. is a guest editor invited by the Editorial Board.

¹To whom correspondence should be addressed. E-mail: hmano@jichi.ac.jp.

This article contains supporting information online at www.pnas.org/cgi/content/full/0805381105/DCSupplemental.

© 2008 by The National Academy of Sciences of the USA

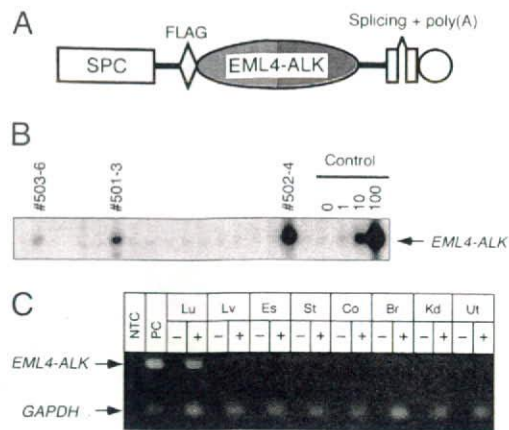


Fig. 1. Generation of transgenic mouse lines for *EML4-ALK*. (A) A cDNA for FLAG-tagged *EML4-ALK* was inserted between the *SPC* promoter and both splicing and polyadenylation [poly(A)] signal sequences. (B) Genomic DNA was isolated from the tail of founder mice generated from pronuclear-stage C57BL/6J embryos and was subjected to Southern blot analysis with full-length *EML4-ALK* cDNA as a probe. Control samples on the right comprised mouse genomic DNA with 0, 1, 10, or 100 copies of the transgene per diploid genome. The ID numbers of founder mice positive for the transgene are shown at the top. (C) Oligo(dT)-primed cDNA was synthesized from total RNA isolated from lung (Lu), liver (Lv), esophagus (Es), stomach (St), colon (Co), brain (Br), kidney (Kd), and uterus (Ut) of an F₁ mouse of the 502-4 line, with the reaction being performed in the presence (+) or absence (–) of reverse transcriptase. The cDNA preparations were then subjected to PCR with primer sets for *EML4-ALK* or for *GAPDH*, and the PCR products were separated by agarose gel electrophoresis and stained with ethidium bromide. The positions of the PCR products are indicated on the left. RT-PCR was also performed for a no-template control (NTC) and for a human NSCLC specimen harboring *EML4-ALK* variant 1 as a positive control (PC).

examination revealed hundreds of nodules in both lungs of this animal (Fig. 2A) and that these nodules were filled with adenocarcinoma cells (Fig. 2B). Immunohistochemical analysis with antibodies to ALK showed a diffuse cytoplasmic staining with granular accentuations in the neoplastic cells (Fig. 2C), consistent with the results of a similar analysis of *EML4-ALK*-positive human tumors (16). The level of immunoreactivity in the lungs of the transgenic mouse, however, was substantially lower than that in *EML4-ALK*-positive human specimens, suggestive of a lower level of expression for the *EML4-ALK* protein.

Detection of *EML4-ALK* by immunoblot analysis with antibodies to the FLAG tag confirmed a low-level but lung-specific expression of the kinase (Fig. 2D). Pathology and computed tomography (CT) examinations (see below) of the progeny of the maintained transgenic mouse lines (501-3 and 502-4) also revealed the development of multiple adenocarcinoma nodules in their lungs at only a few weeks after birth, demonstrating an essential role for the *EML4-ALK* kinase in NSCLC carcinogenesis. There was no discernable difference in tumor-forming activity between the 2 transgenic lines. We thus used both of these lines for further analyses.

Treatment of NSCLC-Positive Transgenic Mice with an ALK-Specific Inhibitor.

To observe the development of NSCLC in the transgenic mice, we performed a series of CT scans of the chest. Multiple large nodules, some with infiltrative profiles of NSCLC, were detected in the lungs of progeny mice [Fig. 3A; also see supporting information (SI) Movie S1]. Other progeny with similar CT findings were subjected to pathology examination, confirming that such CT profiles reflected tumor expansion and infiltration in the lungs (data not shown). Examination of other organs of these mice failed to detect metastatic tumor nodules.

Several chemical compounds that specifically inhibit the ty-

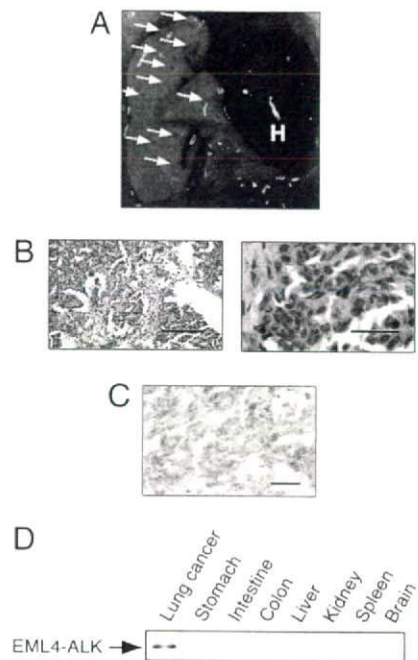


Fig. 2. Development of lung adenocarcinoma in *EML4-ALK* transgenic mice. (A) Hundreds of adenocarcinoma nodules (arrows) were apparent in the lungs of a founder mouse (503-6) that died 3 weeks after birth. H, heart. (B) Microscopic examination of the nodules shown in A after staining with H&E. Images at low (Left) and high (Right) magnification are shown with scale bars of 200 and 40 μ m, respectively. Some tumors exhibited obvious scar formation, suggesting that they were invasive carcinomas. (C) Immunohistochemical analysis with antibodies to ALK of one of the nodules shown in A revealed a pattern of cytoplasmic staining with granular accentuations. (Scale bar, 50 μ m.) (D) Immunoprecipitates prepared with antibodies to FLAG from the indicated tissues of an F₁ mouse of the 502-4 line were subjected to immunoblot analysis with the same antibodies. The position of *EML4-ALK* is shown at the left.

rosine kinase activity of ALK have been identified (17–19). One such 2,4-pyrimidinediamine derivative has a median inhibitory concentration for ALK of <10 nM and a high specificity to ALK (Fig. S1) (20). We therefore examined whether peroral treatment with this compound (10 mg per kg of body weight per day) might inhibit the growth or induce the death of the adenocarcinoma cells in the transgenic mice. CT scans were performed after 0, 11, and 25 days of treatment for all 10 mice in each of the treatment and control (vehicle) groups, and a sequential examination of CT profiles was undertaken for each animal. The tumor mass developed rapidly in both lungs for most of the animals in the control group (Fig. 3A; also see Movie S2). Multiple nodules of various sizes newly appeared in the lungs, and the existing nodules became enlarged. In contrast, treatment with the ALK inhibitor greatly reduced the tumor burden in all mice (Fig. 3B). A large tumor in the lower lobe of the right lung in mouse 373, for instance, was reduced to \approx 30% of its original size (based on the cross-section at the chest level in Fig. 3B) after only 11 days of the drug treatment and was almost undetectable by CT after treatment for 25 days (Movie S3). Sequential CT examination of another mouse (381) confirmed the pronounced activity of the ALK inhibitor (Fig. 3B; also see Movie S4 and Movie S5).

Mice in both groups were killed for pathology analysis after drug or vehicle administration for 2 months. Although multiple large tumor nodules were readily identified in the lungs of control mice, such nodules were apparent only occasionally in the treated animals (Fig. 3C), confirming the marked therapeutic effect of the ALK inhibitor. However, several small nodules were detected in the

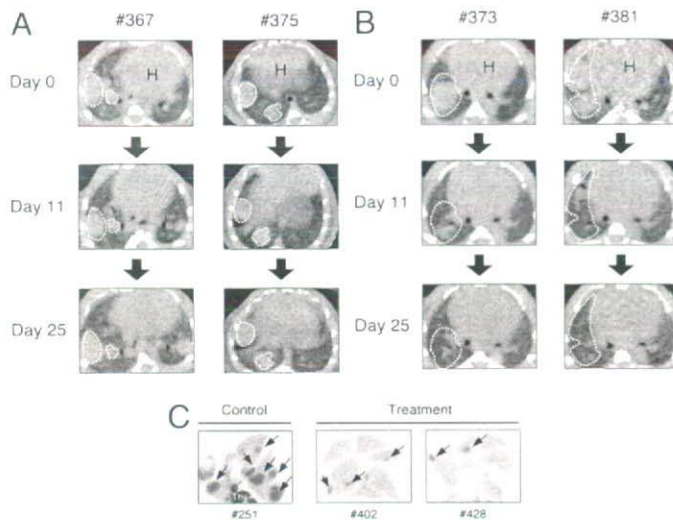


Fig. 3. Treatment of *EML4-ALK* transgenic mice with a specific ALK inhibitor. (A and B) Transgenic mice were subjected to daily peroral administration of vehicle (A) or ALK inhibitor (B) beginning at 4 weeks of age and were examined by CT scanning of the chest on days 0, 11, and 25. The ID numbers of the mice are shown at the top. H, heart. Tumors (indicated by broken lines) in both lungs underwent progressive enlargement in all control mice but became progressively smaller in all treated animals. (C) Macroscopic examination of the lungs from mice of the control and treatment groups at 2 months after the onset of treatment. The tissue was stained with H&E. The ID numbers of the mice are shown at the bottom. Cancer nodules are indicated by arrows. Thy, thymus.

treated mice. Microscopic examination of the lungs of control and treated mice confirmed the changes observed by CT scanning and macroscopic analysis (data not shown). Even at this time point, we did not detect metastatic nodules in organs other than the lungs in either control or treated mice, and all animals in these cohorts survived the observation period.

Treatment of Mice Injected with 3T3 Cells Expressing *EML4-ALK*.

Given that transgenic mice with lung cancer did not die by 6 months of age (with the exception of the one shown in Fig. 2A and another that died at 6 months after birth), we were not able to examine statistically the possible effect of the ALK inhibitor on survival in these animals. We therefore adopted another approach—that of loading mice with a large number of *EML4-ALK*-positive cells. We previously showed that mouse 3T3 fibroblasts expressing *EML4-ALK* (*EML4-ALK/3T3*) undergo transformation and generate s.c. tumors when injected into *nu/nu* mice (12). Such *EML4-ALK/3T3* cells (2×10^5) were therefore injected i.v. into *nu/nu* mice ($n = 20$), and the ALK inhibitor was administered to half of these animals.

A total of 9 of the 10 untreated mice died within 1 month of injection with the *EML4-ALK/3T3* cells (Fig. 4A). Postmortem examination of these mice revealed extensive dissemination of *EML4-ALK*-positive cells into the lungs (>60% of lung tissue was occupied with the transformed *EML4-ALK/3T3* cells in all mice) (Fig. 4B). Pathology examination of the lungs revealed many nodules of various sizes that were filled with the *EML4-ALK/3T3* fibroblasts (Fig. 4C). In a separate experiment, we confirmed that injection of parental 3T3 cells did not induce the formation of such nodules in the lungs or affect the survival of mice (data not shown).

To verify that the injected *EML4-ALK/3T3* cells continued to express *EML4-ALK*, we stained tissue sections of the lungs of control mice with antibodies to ALK. All cells within nodules reacted with the antibodies (Fig. 4D), giving rise to a diffuse pattern of cytoplasmic staining with granular accentuations. Although the staining profile was similar to that observed for the transgenic mice,

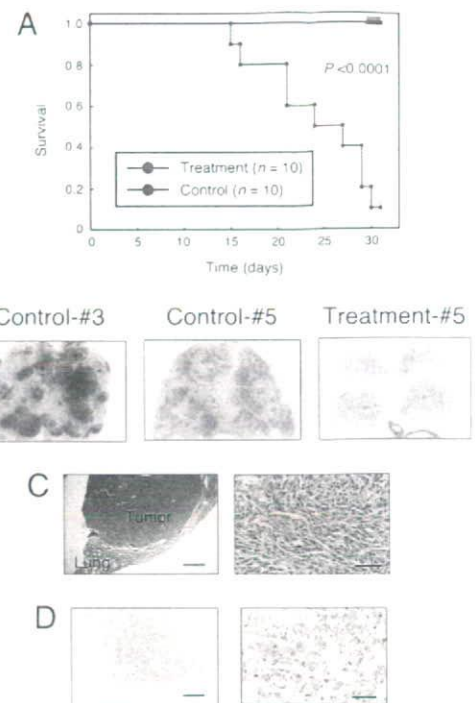


Fig. 4. Treatment with the ALK inhibitor of mice injected with *EML4-ALK/3T3* cells. (A) Nude mice were injected i.v. with 2×10^5 3T3 cells expressing *EML4-ALK* variant 1 and were then immediately subjected to daily peroral administration of vehicle (control, $n = 10$) or ALK inhibitor (treatment, $n = 10$). Survival of the 2 cohorts is shown as a Kaplan-Meier plot and was compared by the log-rank test, with the calculated *P* value indicated. (B) Macroscopic examination of lungs isolated from mice of the control group at death or of the treatment group after treatment for 31 days. The tissue was stained with H&E. Most of the lungs in both control animals were occupied with transformed *EML4-ALK/3T3* cells, whereas such cells were rarely observed in the treated animal. (C) Microscopic examination of lung tissue from a mouse of the control group after H&E staining. Images of low (Left) and high (Right) magnification are shown with scale bars of 500 and 50 μm , respectively. (D) Immunohistochemical analysis with antibodies to ALK of the nodules of *EML4-ALK/3T3* cells that formed in the lungs of a mouse in the control group. Images of low (Left) and high (Right) magnification are shown with scale bars of 200 and 50 μm , respectively.

the staining intensity in the *EML4-ALK/3T3* cell-injected animals was greater than that in the transgenic animals.

Similar to the results obtained with transgenic mice, transformed *EML4-ALK/3T3* cells were not detected in any organs other than the lungs of the injected mice, with the exception of 2 animals in the control group (nos. 3 and 7). Given the massive infiltration of *EML4-ALK/3T3* cells in the lungs of all mice in the control cohort, these mice likely died from respiratory failure. In the control no. 7 mouse, we detected pronounced infiltration of *EML4-ALK/3T3* cells into both the mediastinum (Fig. S2A) and the diaphragm (Fig. S2B). Given that both of these structures are adjacent to the lungs and that this mouse had an exceptionally high tumor burden in the lungs (>90% of the lungs were occupied with *EML4-ALK/3T3* cells; Fig. S2C), the presence of *EML4-ALK/3T3* cells in the mediastinum and diaphragm was likely the result of direct invasion from the lungs rather than of distant metastasis.

Peroral administration of the ALK inhibitor markedly improved the outcome of mice injected with the transformed *EML4-ALK/3T3* cells, with all 10 animals in the treatment group surviving the 1-month observation period ($P < 0.0001$, log-rank test) (Fig. 4A). The treated mice also were subjected to pathology analysis after this period, revealing the absence of *EML4-*

ALK/3T3 nodules from the lungs (Fig. 4B) and again demonstrating the high efficacy of the ALK inhibitor.

Discussion

We have shown here that the EML4-ALK fusion kinase plays an essential role in lung tumorigenesis. Hundreds of adenocarcinoma nodules developed simultaneously within a few weeks after birth in all independent lines of *EML4-ALK* transgenic mice examined. Given that the promoter fragment of *SPC* becomes active only at a late stage of gestation (21), a short period of *EML4-ALK* expression appears to be sufficient for full transformation. Although we did not examine *TP53* and *RBI* for possible abnormalities in the adenocarcinoma nodules of the transgenic mice, with both of these genes being frequently inactivated in human lung cancers (22), it is likely that only one (or at most a few) additional genetic event is required to generate cancer in EML4-ALK-expressing alveolar epithelial cells.

The expression level of EML4-ALK protein in the adenocarcinoma nodules of the transgenic mice was low. Given that the abundance of *EML4-ALK* mRNA in these nodules was found to be greater than that in human *EML4-ALK*-positive NSCLC specimens (data not shown), the expression of EML4-ALK protein appears to be suppressed in the mouse lung epithelial cells, possibly through translational or posttranslational mechanisms. The development of adenocarcinoma even at this low level of protein expression further reinforces the transforming activity of EML4-ALK.

Given the rapid development of NSCLC induced by EML4-ALK, the tumor cells are likely dependent for growth on the tyrosine kinase activity of the fusion protein. Such "oncogene addiction" (23) provides a potential target for the development of treatment strategies. We therefore tested whether inhibition of the enzymatic activity of EML4-ALK might reduce the tumor burden in the transgenic mice. The ALK inhibitor examined proved to be a promising candidate for the treatment of EML4-ALK-positive tumors. Furthermore, given the high sensitivity of the tumors in the transgenic mice to the ALK inhibitor, these animals provide a model system with which to examine the *in vivo* activity of other compounds or reagents targeted to ALK.

Many of the large tumors in the lungs of the transgenic mice changed to bullae or cysts after treatment with the ALK inhibitor, as revealed both by CT scanning (Fig. S3A and Movie S3 and Movie S5) and by pathology examination (Fig. S3B). Such a change was not described for treatment of activated EGFR-positive NSCLC in mouse models or humans with EGFR inhibitors (5, 6). A rapid induction of cell death by the ALK inhibitor in the transgenic mice may have triggered a collapse of the tumor burden within each nodule, thereby giving rise to bullae or cysts. Indeed, pathology examination revealed that a large tumor in 1 transgenic mouse (no. 250) became filled with necrotic tissue after treatment (Fig. S3C). However, the bullae cysts and necrotic tissue were still surrounded by remaining cancer cells (Fig. S3B and C). Similarly, the lining tissue of some bullae cysts in the treated mice appeared to have a high density in CT scans (Fig. S3A), suggesting that peripheral cancer cells may survive in the nodules. Furthermore, small foci of cancer cells could be identified in the lungs of transgenic mice in the treatment cohort (Fig. 3C). Together, these various observations indicate that the current treatment protocol with the ALK inhibitor did not entirely eliminate tumor cells from the transgenic mice. Indeed, in a separate experiment transgenic mice treated with the 2,4-pyrimidinediamine for 25 days were examined 3 months after cessation of drug administration. Tumors of various sizes regrew in these mice (Fig. S4), indicative of the presence of surviving EML4-ALK-positive cancer cells in the animals after 25 days of drug treatment. Given that we have not tried other protocols or compounds, it remains unknown whether a total cure might be achieved by treatment for a longer period or with a higher dose of the same inhibitor or with a more

potent compound. It is also possible that inhibition of additional signaling pathways, such as those mediated by phosphoinositide 3-kinase, mammalian target of rapamycin, or other protein tyrosine kinases (5, 24), may be required for a complete cure.

Despite the rapid growth of multiple tumors in the lungs of the transgenic mice, we failed to detect distant metastasis of such cancer cells in animals killed for analysis or in those that died within the total observation period of 6 months. However, we conclude that the tumors that developed in these mice had malignant characteristics on the basis of the following observations: (i) Histological analysis indicated that most tumors were noninvasive papillary adenocarcinomas, with some of them further showing obvious fibrosis and destruction of alveolar structures (Fig. 2B), a marker of invasion in human lung adenocarcinoma. (ii) Subcutaneous transplantation of tumor nodules that developed in the transgenic mice into the shoulder of *nu/nu* mice resulted in the growth of tumors at 6 of 8 injection sites in the recipient animals (Fig. S5A). (iii) Tumors that developed in the transgenic mice were shown to keep growing for at least 62 days in *in vitro* culture (Fig. S5B).

It is likely that expression of EML4-ALK (and probably other accompanying genetic changes) alone is not sufficient to render the cancer cells metastatic. It remains to be determined whether additional abnormalities in other oncogenes or tumor suppressor genes, such as *KRAS* or *LKB1* (25, 26), may lead to the generation of metastatic tumors in *EML4-ALK* transgenic mice.

Our present results have reinforced the importance of *EML4-ALK* in the pathogenesis of NSCLC in humans and have provided experimental support for the treatment of such intractable tumors with ALK inhibitors. Given that variants of *EML4-ALK* other than the variants 1 and 2 described in our original study (12) are now being identified (20, 27–29), it will be important to characterize all possible isoforms of *EML4-ALK* in humans to identify precisely the subgroup of patients who are candidates for future treatment with ALK inhibitors. Further to this goal, it will also be important to clarify the genetic changes that accompany the *EML4-ALK* fusion event as well as the downstream targets of EML4-ALK action in human NSCLC.

Materials and Methods

Generation of Transgenic Mice. A cDNA fragment encoding FLAG epitope-tagged EML4-ALK variant 1 (12) was ligated to the *SPC* promoter as well as to splicing and polyadenylation signals (Fig. 1A). The expression cassette was injected into pronuclear-stage embryos of C57BL/6 mice (PhoenixBio), and the copy number of the transgene was examined by Southern blot analysis with DNA from the tail of founder animals. All animal procedures were performed with the approval of the scientific committee for animal experiments of Jichi Medical University.

For detection of mRNAs derived from *EML4-ALK* and the glyceraldehyde-3-phosphate dehydrogenase gene (*GAPDH*), total RNA was isolated from the organs of transgenic mice with the use of an RNeasy Mini kit (Qiagen) and was subjected to reverse transcription with SuperScript III reverse transcriptase (Invitrogen) and an oligo(dT) primer. Both reverse transcription and subsequent PCR analysis for each gene were performed as described previously (12).

For analysis of EML4-ALK protein in mice, organ homogenates were prepared with an Nonidet P-40 lysis buffer and subjected to immunoprecipitation with mouse monoclonal antibodies to FLAG (Millipore). The resulting precipitates were then subjected to immunoblot analysis with the same antibodies and a SuperSignal chemiluminescence kit (Pierce Biotechnology).

Pathology Examination. For immunohistochemical staining of EML4-ALK in EML4-ALK/3T3 cells, paraffin-embedded sections were depleted of paraffin with xylene, rehydrated with a graded series of ethanol solutions, and stained with mouse monoclonal antibodies to ALK (ALK1; Dako) at a dilution of 1:20 and with an EnVision+DAB system (Dako). The sections were subjected to heat-induced antigen retrieval with Target Retrieval Solution, pH 9.0 (Dako), before exposure to the antibodies. For detection of EML4-ALK in transgenic mice, cryostat sections were fixed with 4% paraformaldehyde in 0.1 M sodium phosphate buffer (pH 7.4) for 10 min, treated with Target Retrieval Solution, pH 9.0, and immunostained with the monoclonal antibodies to ALK and the EnVision+DAB system.

Treatment with ALK Inhibitor. For the experiments based on i.v. administration of EML4-ALK/3T3 cells, the cells (2×10^5) were injected into the tail vein of 4-week-old *nu/nu* mice (Clea Japan). An inhibitor specific for the tyrosine kinase activity of ALK [example 3-39 in the patent application: Garcia-Echeverria C, et al., inventors; Novartis AG, Novartis Pharma GmbH, IRM LLC, applicants (24 Feb 2005). 2,4-Pyrimidinediamines useful in the treatment of neoplastic disease and in inflammatory and immune system disorders. PCT WO 2005016894] was synthesized by Astellas Pharma and was orally administered each day at a dose of 10 mg/kg to the injected mice or to EML4-ALK-transgenic mice. Sequential examination of lung tumors was performed with an X-ray CT apparatus for experimental animals (LCT-100; Aloka).

- Schiller JH, et al. (2002) Comparison of four chemotherapy regimens for advanced non-small-cell lung cancer. *N Engl J Med* 346:92–98.
- Paez JG, et al. (2004) EGFR mutations in lung cancer: Correlation with clinical response to gefitinib therapy. *Science* 304:1497–1500.
- Pao W, et al. (2004) EGF receptor gene mutations are common in lung cancers from “never smokers” and are associated with sensitivity of tumors to gefitinib and erlotinib. *Proc Natl Acad Sci USA* 101:13306–13311.
- Shigematsu H, et al. (2005) Clinical and biological features associated with epidermal growth factor receptor gene mutations in lung cancers. *J Natl Cancer Inst* 97:339–346.
- Li D, et al. (2007) Bronchial and peripheral murine lung carcinomas induced by T790M-L858R mutant EGFR respond to HKI-272 and rapamycin combination therapy. *Cancer Cell* 12:81–93.
- Lynch TJ, et al. (2004) Activating mutations in the epidermal growth factor receptor underlying responsiveness of non-small-cell lung cancer to gefitinib. *N Engl J Med* 350:2129–2139.
- Kris MG, et al. (2003) Efficacy of gefitinib, an inhibitor of the epidermal growth factor receptor tyrosine kinase, in symptomatic patients with non-small cell lung cancer: A randomized trial. *J Am Med Assoc* 290:2149–2158.
- Hatanaka H, et al. (2007) Transforming activity of purinergic receptor P2Y₂, G-protein coupled, 2 revealed by retroviral expression screening. *Biochem Biophys Res Commun* 356:723–726.
- Fujiwara S, et al. (2007) Transforming activity of purinergic receptor P2Y₂, G protein coupled, 8 revealed by retroviral expression screening. *Leuk Lymphoma* 48:978–986.
- Choi YL, et al. (2007) Identification of a constitutively active mutant of JAK3 by retroviral expression screening. *Leuk Res* 31:203–209.
- Besse B, Ropert S, Soria JC (2007) Targeted therapies in lung cancer. *Ann Oncol* 18(suppl 9):ix135–ix142.
- Soda M, et al. (2007) Identification of the transforming EML4-ALK fusion gene in non-small-cell lung cancer. *Nature* 448:561–566.
- Mishra A, Weaver TE, Beck DC, Rothenberg ME (2001) Interleukin-5-mediated allergic airway inflammation inhibits the human surfactant protein C promoter in transgenic mice. *J Biol Chem* 276:8453–8459.
- Duan W, et al. (2002) Lung-specific expression of human mutant p53–273H is associated with a high frequency of lung adenocarcinoma in transgenic mice. *Oncogene* 21:7831–7838.
- Zhao B, et al. (2000) Transgenic mouse models for lung cancer. *Exp Lung Res* 26:567–579.
- Inamura K, et al. (2008) EML4-ALK fusion is linked to histological characteristics in a subset of lung cancers. *J Thorac Oncol* 3:13–17.
- Chiarle R, Voena C, Ambrogio C, Piva R, Inghirami G (2008) The anaplastic lymphoma kinase in the pathogenesis of cancer. *Nat Rev Cancer* 8:11–23.
- McDermott U, et al. (2007) Identification of genotype-correlated sensitivity to selective kinase inhibitors by using high-throughput tumor cell line profiling. *Proc Natl Acad Sci USA* 104:19936–19941.
- Galkin AV, et al. (2007) Identification of NVP-TAE684, a potent, selective, and efficacious inhibitor of NPM-ALK. *Proc Natl Acad Sci USA* 104:270–275.
- Choi YL, et al. (2008) Identification of novel isoforms of the EML4-ALK transforming gene in non-small cell lung cancer. *Cancer Res* 68:4971–4976.
- Korfhagen TR, et al. (1990) Cis-acting sequences from a human surfactant protein gene confer pulmonary-specific gene expression in transgenic mice. *Proc Natl Acad Sci USA* 87:6122–6126.
- Testa JR, et al. (1997) Advances in the analysis of chromosome alterations in human lung carcinomas. *Cancer Genet Cytogenet* 95:20–32.
- Sharma SV, Settleman J (2007) Oncogene addiction: Setting the stage for molecularly targeted cancer therapy. *Genes Dev* 21:3214–3231.
- Engelman JA, et al. (2007) MET amplification leads to gefitinib resistance in lung cancer by activating ERBB3 signaling. *Science* 316:1039–1043.
- Ji H, et al. (2007) LKB1 modulates lung cancer differentiation and metastasis. *Nature* 448:807–810.
- Huang CL, et al. (1998) Mutations of p53 and K-ras genes as prognostic factors for non-small cell lung cancer. *Int J Oncol* 12:553–563.
- Rikova K, et al. (2007) Global survey of phosphotyrosine signaling identifies oncogenic kinases in lung cancer. *Cell* 131:1190–1203.
- Koivunen JP, et al. (2008) EML4-ALK fusion gene and efficacy of an ALK kinase inhibitor in lung cancer. *Clin Cancer Res* 14:4275–4283.
- Takeuchi K, et al. (2008) Multiplex reverse transcription-PCR screening for EML4-ALK fusion transcripts. *Clin Cancer Res* 14:6618–6624.

Oncogenic mutations of ALK kinase in neuroblastoma

Yuyan Chen^{1,2,3*}, Junko Takita^{1,2,3*}, Young Lim Choi^{4*}, Motohiro Kato^{1,3}, Miki Ohira⁵, Masashi Sanada^{2,3,6}, Lili Wang^{2,3,6}, Manabu Soda⁴, Akira Kikuchi⁷, Takashi Igarashi¹, Akira Nakagawara⁵, Yasuhide Hayashi⁸, Hiroyuki Mano^{4,6} & Seishi Ogawa^{2,3,6}

Neuroblastoma in advanced stages is one of the most intractable paediatric cancers, even with recent therapeutic advances¹. Neuroblastoma harbours a variety of genetic changes, including a high frequency of *MYCN* amplification, loss of heterozygosity at 1p36 and 11q, and gain of genetic material from 17q, all of which have been implicated in the pathogenesis of neuroblastoma^{2–5}. However, the scarcity of reliable molecular targets has hampered the development of effective therapeutic agents targeting neuroblastoma. Here we show that the anaplastic lymphoma kinase (ALK), originally identified as a fusion kinase in a subtype of non-Hodgkin's lymphoma (NPM-ALK)^{6–8} and more recently in adenocarcinoma of lung (EML4-ALK)^{9,10}, is also a frequent target of genetic alteration in advanced neuroblastoma. According to our genome-wide scans of genetic lesions in 215 primary neuroblastoma samples using high-density single-nucleotide polymorphism genotyping microarrays^{11–14}, the *ALK* locus, centromeric to the *MYCN* locus, was identified as a recurrent target of copy number gain and gene amplification. Furthermore, DNA sequencing of *ALK* revealed eight novel missense mutations in 13 out of 215 (6.1%) fresh tumours and 8 out of 24 (33%) neuroblastoma-derived cell lines. All but one mutation in the primary samples (12 out of 13) were found in stages 3–4 of the disease and were harboured in the kinase domain. The mutated kinases were autophosphorylated and displayed increased kinase activity compared with the wild-type kinase. They were able to transform NIH3T3 fibroblasts as shown by their colony formation ability in soft agar and their capacity to form tumours in nude mice. Furthermore, we demonstrate that downregulation of *ALK* through RNA interference suppresses proliferation of neuroblastoma cells harbouring mutated *ALK*. We anticipate that our findings will provide new insights into the pathogenesis of advanced neuroblastoma and that *ALK*-specific kinase inhibitors might improve its clinical outcome.

To identify oncogenic lesions in neuroblastoma, we performed a genome-wide analysis of primary tumour samples obtained from 215 neuroblastoma patients using high-density single-nucleotide polymorphism (SNP) arrays (Affymetrix GeneChip 250K *NspI*) (Supplementary Table 1). Twenty-four neuroblastoma-derived cell lines were also analysed (Supplementary Table 2). Interrogating over 250,000 SNP sites, this platform permits the identification of copy number changes at an average resolution of less than 12 kilobases (kb)^{13,14}.

Analysis of this large number of samples, consisting of varying disease stages, permitted us to obtain a comprehensive registry of genomic lesions in neuroblastoma (Supplementary Figs 1 and 2). A gain of chromosomes, often triploid or hyperploid (defined by mean copy number of >2.5), was a predominant feature of neuroblastoma genomes in the lower stages. Ploidy generally correlated with the

clinical stage, where non-hyperploid cases were significantly associated with stage 4 disease ($P = 4.13 \times 10^{-5}$, trend test) (Supplementary Fig. 3 and Supplementary Table 3). 17q gains, frequently in multiple copies ($3 \leq$ copy number <5), were a hallmark of the neuroblastoma genome⁴ and were found in most neuroblastoma cases. Copy number gains tended to spare chromosomes 3, 4, 10, 14 and 19 (Supplementary Figs 2 and 3). Notably, these chromosomes often had copy number losses including 1p (22.8%), 3p (8.8%), 4p (5.1%), 6q (7.0%), 10q (9.8%), 11q (19.5%), 14q (3.7%), 19p (7.4%) and 19q (5.1%), implicating the pathogenic role of 'relative' gene dosages.

After excluding known copy number variations, we identified a total of 28 loci undergoing high-grade amplifications (copy number ≥ 5) (Supplementary Table 4). These lesions fell into relatively small genomic segments, having a mean size of 361 kb, which accelerated the identification of gene targets in these regions (Supplementary Table 4 and Supplementary Fig. 4). The candidate gene targets included *TERT* (5p15.33), *HDAC3* (5q31.3), *IGF2* (11p15.1), *MYEOV* (11q13.3), *FGF7* (15q21.1) and *CDH13* (16q23.3). However, many of them were not recurrent but found only in a single case. Although the recurrent lesions were mostly explained by the amplification of *MYCN* at 2p24, as found in 50 out of 215 (23%) of the primary cases, we identified another peak of recurrent amplification at 2p23 (Fig. 1a), which consisted of amplicons in five primary cases and in one neuroblastoma-derived cell line, NB-1 (Supplementary Fig. 5). This peak was located at the centromeric margin of the common copy number gains in chromosome 2p, which was created by copy number gains in 109 samples mostly from non-hyperploid stage 4 cases. The minimum overlapping amplification was defined by the amplicons found in the NB-1 cell line (Supplementary Fig. 5) and contained a single gene, the anaplastic lymphoma kinase (*ALK*), which has previously been reported to be overexpressed in neuroblastoma cases¹⁵. Although five of the six samples showing *ALK* amplification also had *MYCN* amplification, one primary case (NT056) lacked a *MYCN* peak and the amplification was confined to the *ALK*-containing locus. In interphase fluorescent *in situ* hybridization (FISH) analysis of NB-1, *MYCN* and *ALK* loci were amplified in separate amplicons (Fig. 1b), indicating that the 2p23 amplicons containing *ALK* were unlikely to represent merely 'passenger' events of *MYCN* amplification but actively contributed to the pathogenesis of neuroblastoma.

Because an oncogene can be activated by gene amplification and/or mutation, to search for possible mutations we performed DNA heteroduplex formation analysis¹⁶ and genomic DNA sequencing for the exons 20 to 28 of *ALK*, which encompass the juxtamembrane and kinase domains (Supplementary Table 5). In total, we identified eight nucleotide changes in 21 neuroblastoma samples, 13 out of 215

¹Department of Pediatrics, ²Cell Therapy and Transplantation Medicine, ³Cancer Genomics Project, Graduate School of Medicine, The University of Tokyo, Tokyo 113-8655, Japan.

⁴Division of Functional Genomics, Jichi Medical University, Tochigi 329-0498, Japan. ⁵Division of Biochemistry, Chiba Cancer Center Research Institute, Chiba 260-8717, Japan.

⁶Core Research for Evolutional Science and Technology, Japan Science and Technology Agency, Saitama, 332-0012, Japan. ⁷Division of Hematology/Oncology, Saitama Children's

Medical Center, Saitama 339-8551, Japan. ⁸Gunma Children's Medical Center, Shibukawa 377-8577, Japan.

*These authors contributed equally to this work.

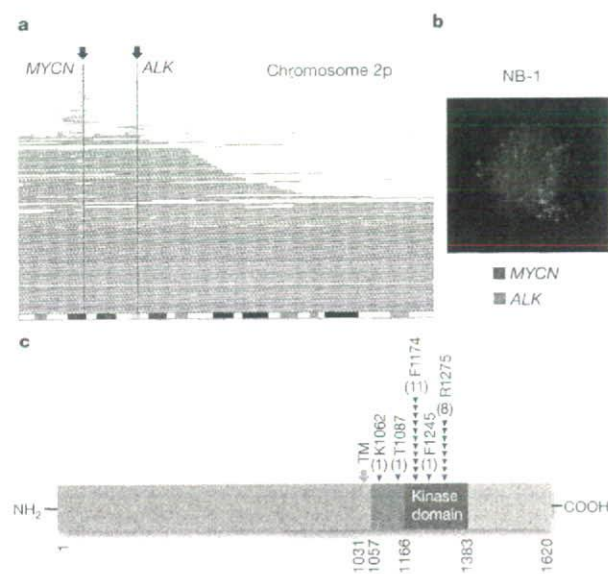


Figure 1 | Common 2p gains/amplifications and *ALK* mutations in neuroblastoma samples. **a**, Recurrent copy number gains on the 2p arm. High-grade amplifications are shown by light-red horizontal lines, whereas simple gains are shown by dark-red lines. Two common peaks of copy number gains and amplifications in the *MYCN* and *ALK* loci are indicated by arrows. The cytobands in 2p are shown at the bottom. **b**, Interphase FISH analysis of NB-1 showing high-grade amplification of *MYCN* (red) and *ALK* loci (green). The amplified *MYCN* locus appears as a single large signal. **c**, Distribution of the eight *ALK* mutations found in 21 neuroblastoma samples. The positions of the mutated amino acids are indicated by black (primary samples) and red (cell lines) arrowheads. The number of mutations at each site is shown at the top of the arrowheads. TM, transmembrane.

(6.1%) primary samples and 8 out of 24 (33%) cell lines, which resulted in seven types of amino acid substitutions at five different positions (Table 1 and Supplementary Fig. 6). They were not found in either the genomic DNA collected from 50 healthy volunteers or in the SNP databases at the time of preparing this manuscript. In fact, somatic origins of missense changes were confirmed in 9 out of 13 primary cases, for which DNA was obtained from the peripheral blood or the tumour-free bone marrow specimens (Supplementary Fig. 6). On the other hand, T1087I (ACC>ATC), found in case NT126, had a germline origin and thus it could not be determined whether the T1087I change was a rare non-functional polymorphism or represented a pathogenic germline mutation. For other changes found in three primary cases (NT128, NT217 and NT218) and cell lines, normal DNA was not available but they were likely to represent oncogenic mutations because they were identical to common somatic changes (F1174L or R1275Q) or shown to have oncogenic potential in functional assays (K1062M).

Most mutations occurred within the kinase domain (20 out of 22 or 91%), which clearly showed two mutation hotspots at F1174 and R1275 (Fig. 1c). A neuroblastoma-derived cell line, SJNB-2, had a homozygous *ALK* mutation of R1275Q, which was probably due to uniparental disomy of chromosome 2 (Supplementary Fig. 7a). Another case (NT074) harboured two different mutations, F1174L and R1275Q, but it remains to be determined whether both are on the same allele. *ALK* mutations within the kinase domain occurred at amino acid positions that are highly conserved across species and during molecular evolution (Supplementary Figs 8 and 9). According to the conserved structure of other insulin receptor kinases we predicted that F1174 is located at the end of the C α 1 helix, whereas the other two are on the two β -sheets: before the catalytic loop (β 6, F1245) and within the activation loop (β 9, R1275) (Supplementary Fig. 7b, c)¹⁷. Thus, conformational changes due to amino acid substitutions at these positions might be responsible for the aberrant activity of the mutant kinases.

Table 1 | *ALK* mutations/amplifications in neuroblastoma samples

| Sample | Age (months) | Stage | <i>MYCN</i> * | Clinical outcome | Mutations/amplifications | Nucleotide substitution | Origin of mutations |
|----------|--------------|-------|---------------|------------------|--------------------------|-------------------------|---------------------|
| NT126 | 99 | 4 | - | Dead | T1087I | ACC>ATC | Germline |
| NT218 | 8 | 1 | - | Alive | F1174L | TTC>TTG | ND |
| NT074 | 34 | 3 | + | Dead | F1174L R1275Q | TTC>TTA CGA>CAA | Somatic |
| NT160 | 12 | 4 | + | Dead | F1174L | TTC>TTA | Somatic |
| NT217 | 24 | 4 | + | Dead | F1174L | TTC>TTA | ND |
| NT190 | 48 | 4 | + | Alive | F1174L | TTC>TTA | Somatic |
| NT060 | 163 | 3 | - | Alive | F1174C | TTC>TGC | Somatic |
| NT162 | 28 | 4 | + | Dead | F1174V | TTC>GTC | Somatic |
| NT195 | 24 | 4 | + | Alive | F1245L | TTC>TTG | Somatic |
| NT055 | 6 | 3 | - | Alive | R1275Q | CGA>CAA | Somatic |
| NT128 | 8 | 4 | - | Dead | R1275Q | CGA>CAA | ND |
| NT164 | 54 | 4 | + | Dead | R1275Q | CGA>CAA | Somatic |
| NT200 | 133 | 4 | - | Dead | R1275Q | CGA>CAA | Somatic |
| SCMC-N5† | - | - | + | - | K1062M | AAG>ATG | ND |
| SJNB-4† | - | - | + | - | F1174L | TTC>TTA | ND |
| LAN-1† | - | - | + | - | F1174L | TTC>TTA | ND |
| SCMC-N2† | - | - | + | - | F1174L | TTC>TTA | ND |
| SK-N-SH† | - | - | + | - | F1174L | TTC>TTA | ND |
| SJNB-2†‡ | - | - | + | - | R1275Q | CGA>CAA | ND |
| LAN-5† | - | - | + | - | R1275Q | CGA>CAA | ND |
| TGW† | - | - | + | - | R1275Q | CGA>CAA | ND |
| NT204 | 12 | 1 | + | Alive | Amplification | - | - |
| NT056 | 11 | 3 | - | Dead | Amplification | - | - |
| NT071 | 36 | 3 | + | Alive | Amplification | - | - |
| NT165 | 19 | 4 | + | Dead | Amplification | - | - |
| NT169 | 7 | 4 | + | Dead | Amplification | - | - |
| NB-1† | - | - | + | - | Amplification | - | - |

ND, not determined.

* Presence (+) or absence (-) of *MYCN* amplification in FISH analysis. All cases where there was an absence of *MYCN* amplification (-) were also checked for possible *MYCN* mutations by sequencing of all *MYCN* exons, but no *MYCN* mutations were identified.

† Cell lines

‡ Homozygous mutation.

ALK mutation highly correlated with MYCN amplification ($P = 1.55 \times 10^{-4}$, Fisher's exact test; Supplementary Table 6) where 14 out of 21 mutations coexisted with MYCN amplification. Regardless of the status of MYCN amplification, 12 of the 13 mutations were found in patients with advanced stage neuroblastoma (Table 1). However, whereas MYCN amplification and stage 4 were significant risk factors for poor survival, the mutation/amplification status of ALK was not likely to have a major impact on survival (Supplementary Fig. 10 and Supplementary Table 7), although the statistical power of the current analysis was largely limited in order to detect a marginal hazard.

To evaluate the impact of ALK mutations on kinase activity, we generated Flag-tagged constructs of ALK and its mutants, F1174L and K1062M, which were stably expressed in NIH3T3 cells, and examined their phosphorylation status and *in vitro* kinase activity. The ALK mutants stably expressed in NIH3T3 cells were phosphorylated according to western blot analysis using an antibody specific for phosphorylated ALK (anti-pY1604) and a PY20 blot after anti-Flag immunoprecipitation of the mutant kinases (Fig. 2a), whereas the wild-type kinase was not phosphorylated. The immunoprecipitated ALK mutants also showed increased tyrosine kinase activity *in vitro* when compared with wild-type ALK. This was shown using both a universal substrate for tyrosine kinase (poly-GluTyr) and the synthetic YFF peptide¹⁸, which was derived from a sequence of the

activation loop of ALK (Fig. 2b, c). In accordance with these findings, downstream molecules of ALK signalling including AKT, STAT3 and ERK¹⁵ were activated in cells expressing mutant ALK, as shown by their increased phosphorylation (Fig. 2d).

Next, we investigated the oncogenic potential of these mutants. NIH3T3 cells stably expressing mutant kinases showed increased colony formation in soft agar compared with the wild-type protein (Fig. 3a and Supplementary Fig. 11). The tumorigenicity of these ALK mutants was further assayed by injecting 1.0×10^7 NIH3T3 cells into nude mice. The NIH3T3 cells transfected with the ALK mutants showed focus-forming capacity and developed subcutaneous tumours (6 out of 6 inoculations) 21 days after inoculation, whereas the mock and wild-type ALK-transfected cells did not (0 out of 6 inoculations) (Fig. 3b, c). Finally, we examined the effect of ALK inhibition on the proliferation of neuroblastoma-derived cell lines. RNA interference (RNAi)-mediated ALK knockdown resulted in reduced cell proliferation of SK-N-SH cells harbouring the F1174L mutation, but the effects were less clear in wild-type ALK-expressing LAN-2 cells (Fig. 3d, e). Of particular interest is a recent report that 5 out of 17 neuroblastoma-derived cell lines, including SK-N-SH and NB-1, frequently showed high sensitivity to the specific ALK inhibitor TAE684 (ref. 19).

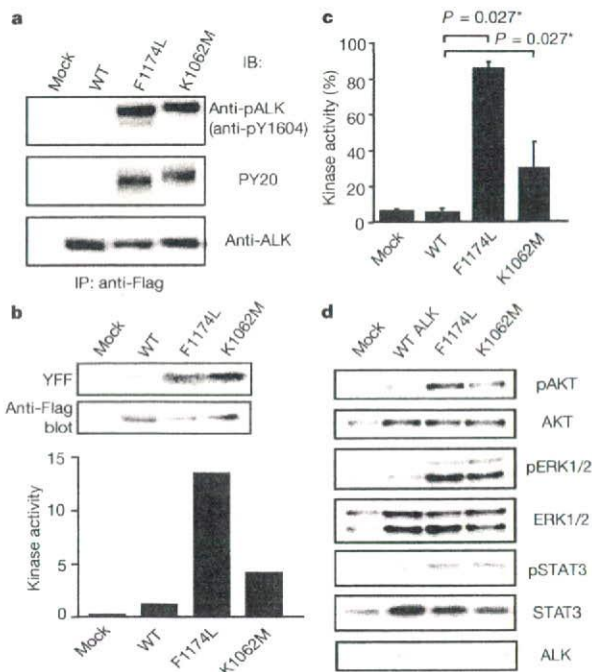


Figure 2 | Kinase activity of ALK mutants and their downstream signalling. **a**, Stably expressed ALK and its mutants (F1174L and K1062M) were immunoprecipitated with an anti-Flag antibody and subjected to western blot analysis with anti-pY1604 (upper panel) or PY20 (middle panel). An anti-ALK blot of precipitated kinases is also displayed (bottom panel). **b**, *In vitro* kinase assay for wild-type ALK kinase and its mutants using the synthetic YFF peptide as a substrate, where kinase activity is expressed as relative values to that for wild-type kinase based on the densities in the autoradiogram. **c**, Kinase activity was also assayed for the poly-GluTyr peptide. Significantly different measurements are indicated by asterisks with *P* values. Bars show mean (\pm s.d.) in three independent experiments. **d**, Western blot analyses of NIH3T3 cells expressing wild-type and mutant ALK for phosphorylated forms of AKT (pAKT), ERK (pERK1/2) and STAT3 (pSTAT3). The total amount of each molecule is also displayed (AKT, ERK1/2, and STAT3) together with an anti-ALK blot (ALK).

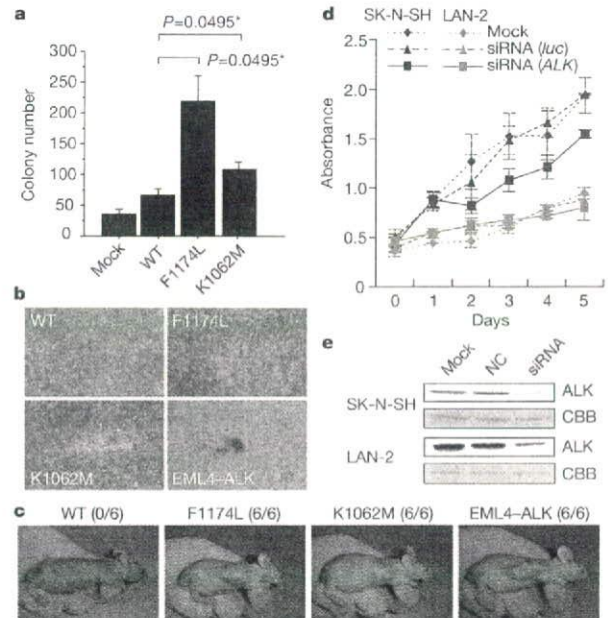


Figure 3 | Oncogenic role of ALK mutations. **a**, Colony assays for NIH3T3 cells stably expressing wild-type as well as mutant ALK (F1174L and K1062M). The average numbers of colonies in triplicate experiments are plotted and standard deviation is indicated. Results showing statistically significant differences as compared with experiments using wild-type ALK are indicated by asterisks with *P* values. **b**, **c**, NIH3T3 cells were transfected with wild-type and mutant ALK (F1174L, K1062M and EML4-ALK) and subjected to a focus forming assay (**b**) as well as an *in vivo* tumorigenicity assay in nude mice (**c**). **d**, Effect of RNAi-mediated ALK knockdown on cell proliferation in neuroblastoma cell lines expressing either the F1174L mutant (SK-N-SH) or wild-type ALK (LAN-2). Cell growth was measured using the Cell Counting Kit-8 after knockdown experiments using ALK-specific siRNAs (siRNA ALK), control siRNAs (siRNA luc), or mock experiments, where absorbance was measured in triplicate and averaged for each assay. To draw growth curves, the mean \pm s.d. of the averaged absorbance in three independent knockdown experiments is plotted. **e**, Successful knockdown of ALK protein was confirmed by anti-ALK blots (ALK) using Coomassie brilliant blue G-250 (CBB) staining as loading controls. NC, control siRNA; siRNA, ALK siRNA.

Through the genome-wide analysis of genetic lesions in neuroblastoma, we identified novel oncogenic *ALK* mutations in advanced neuroblastoma. Combined with the cases having a high-grade amplification of the *ALK* gene, aberrant *ALK* signalling was likely to be involved in 11% (16 out of 151) of the advanced neuroblastoma cases. Because *ALK* kinase has been shown to be deregulated only in the form of a fusion kinase in human cancers, including lymphoma and lung cancer, the identification of oncogenic mutations in *ALK* not only increases our understanding of the molecular pathogenesis of advanced neuroblastoma, but also adds a new paradigm to the concept of 'ALK-positive human cancers' in that the mutated *ALK* kinases themselves might participate in human cancers. Our results again highlight the power of genome-wide studies to clarify the genetic lesions in human cancers^{20–22}. Given that *ALK* mutations are preferentially involved in advanced neuroblastoma cases having a poor prognosis, our findings implicate that *ALK* inhibitors may improve the clinical outcome of children suffering from intractable neuroblastoma.

METHODS SUMMARY

Genomic DNA from 215 patients with primary neuroblastoma and 24 neuroblastoma-derived cell lines was analysed on GeneChip SNP genotyping microarrays (Affymetrix GeneChip 250K NspI). After appropriate normalization of mean array intensities, signal ratios were calculated between tumours and anonymous normal references in an allele-specific manner, and allele-specific copy numbers were inferred from the observed signal ratios based on the hidden Markov model using CNAG/AsCNAR software^{13,14}. *ALK* mutations were examined by DNA heteroduplex analysis and/or genomic DNA sequencing¹⁵. Full-length cDNAs for mutant *ALK* were isolated by high-fidelity PCR and inserted into pcDNA3 and pMXS. The expression plasmids were transfected into NIH3T3 cells using Effectene Transfection Reagent (Qiagen) or by calcium phosphate methods⁹. Western blot analysis of mutant *ALK* kinases, *in vitro* kinase assays, and tumour formation assays in nude mice were performed as previously described⁹. This study was approved by the ethics boards of the University of Tokyo and of the Chiba Cancer Center Research Institute.

Full Methods and any associated references are available in the online version of the paper at www.nature.com/nature.

Received 3 June; accepted 28 August 2008.

- Maris, J. M., Hogarty, M. D., Bagatell, R. & Cohn, S. L. Neuroblastoma. *Lancet* **369**, 2106–2120 (2007).
- Maris, J. M. *et al.* Loss of heterozygosity at 1p36 independently predicts for disease progression but not decreased overall survival probability in neuroblastoma patients: a Children's Cancer Group study. *J. Clin. Oncol.* **18**, 1888–1899 (2000).
- Attiyeh, F. F. *et al.* Chromosome 1p and 11q deletions and outcome in neuroblastoma. *N. Engl. J. Med.* **353**, 2243–2253 (2005).
- Bown, N. *et al.* Gain of chromosome arm 17q and adverse outcome in patients with neuroblastoma. *N. Engl. J. Med.* **340**, 1954–1961 (1999).
- Brodeur, G. M., Seeger, R. C., Schwab, M., Varmus, H. E. & Bishop, J. M. Amplification of *N-myc* in untreated human neuroblastomas correlates with advanced disease stage. *Science* **224**, 1121–1124 (1984).
- Shiota, M. *et al.* Anaplastic large cell lymphomas expressing the novel chimeric protein p80NPM/ALK: a distinct clinicopathologic entity. *Blood* **86**, 1954–1960 (1995).
- Morris, S. W. *et al.* Fusion of a kinase gene, *ALK*, to a nucleolar protein gene, *NPM*, in non-Hodgkin's lymphoma. *Science* **263**, 1281–1284 (1994).
- Fujimoto, J. *et al.* Characterization of the transforming activity of p80, a hyperphosphorylated protein in a Ki-1 lymphoma cell line with chromosomal translocation t(2;5). *Proc. Natl. Acad. Sci. USA* **93**, 4181–4186 (1996).
- Soda, M. *et al.* Identification of the transforming *EML4-ALK* fusion gene in non-small-cell lung cancer. *Nature* **448**, 561–566 (2007).
- Rikova, K. *et al.* Global survey of phosphotyrosine signaling identifies oncogenic kinases in lung cancer. *Cell* **131**, 1190–1203 (2007).
- Kennedy, G. C. *et al.* Large-scale genotyping of complex DNA. *Nature Biotechnol.* **21**, 1233–1237 (2003).
- Matsuzaki, H. *et al.* Genotyping over 100,000 SNPs on a pair of oligonucleotide arrays. *Nature Methods* **1**, 109–111 (2004).
- Nannya, Y. *et al.* A robust algorithm for copy number detection using high-density oligonucleotide single nucleotide polymorphism genotyping arrays. *Cancer Res.* **65**, 6071–6079 (2005).
- Yamamoto, G. *et al.* Highly sensitive method for genomewide detection of allelic composition in nonpaired, primary tumor specimens by use of affymetrix single-nucleotide-polymorphism genotyping microarrays. *Am. J. Hum. Genet.* **81**, 114–126 (2007).
- Osajima-Hakomori, Y. *et al.* Biological role of anaplastic lymphoma kinase in neuroblastoma. *Am. J. Pathol.* **167**, 213–222 (2005).
- Donohoe, E. Denaturing high-performance liquid chromatography using the WAVE DNA fragment analysis system. *Methods Mol. Med.* **108**, 173–187 (2005).
- Hu, J., Liu, J., Ghirlando, R., Saltiel, A. R. & Hubbard, S. R. Structural basis for recruitment of the adaptor protein APS to the activated insulin receptor. *Mol. Cell* **12**, 1379–1389 (2003).
- Donella-Deana, A. *et al.* Unique substrate specificity of anaplastic lymphoma kinase (ALK): development of phosphoacceptor peptides for the assay of ALK activity. *Biochemistry* **44**, 8533–8542 (2005).
- McDermott, U. *et al.* Genomic alterations of anaplastic lymphoma kinase may sensitize tumors to anaplastic lymphoma kinase inhibitors. *Cancer Res.* **68**, 3389–3395 (2008).
- Garraway, L. A. *et al.* Integrative genomic analyses identify *MET* as a lineage-survival oncogene amplified in malignant melanoma. *Nature* **436**, 117–122 (2005).
- Mullighan, C. G. *et al.* Genome-wide analysis of genetic alterations in acute lymphoblastic leukaemia. *Nature* **446**, 758–764 (2007).
- Kawamata, N. *et al.* Molecular allelotyping of pediatric acute lymphoblastic leukemias by high-resolution single nucleotide polymorphism oligonucleotide genomic microarray. *Blood* **111**, 776–784 (2008).

Supplementary Information is linked to the online version of the paper at www.nature.com/nature.

Acknowledgements We thank H. P. Koeffler for critically reading and editing the manuscript. We also thank M. Matsumura, Y. Ogino, S. Ichimura, S. Sohma, E. Matsui, Y. Yin, N. Hoshino and Y. Nakamura for their technical assistance. This work was supported by the Core Research for Evolutional Science and Technology, Japan Science and Technology Agency and by a Grant-in-Aid from the Ministry of Health, Labor and Welfare of Japan for the third-term Comprehensive 10-year Strategy for Cancer Control.

Author Contributions Y.C., Y.L.C. and J.T. contributed equally to this work. M.K. and M.Sa. performed microarray experiments and subsequent data analyses. Y.C. and J.T. performed mutation analysis of *ALK*. Y.C., Y.L.C., J.T., M.Sa., L.W. and H.M. conducted functional assays of mutant *ALK*. A.N., M.O., T.I., A.K. and Y.H. prepared tumour specimens and were involved in statistical analysis. A.N., Y.H., H.M., J.T. and S.O. designed the overall study, and S.O. and J.T. wrote the manuscript. All authors discussed the results and commented on the manuscript.

Author Information The nucleotide sequences of *ALK* mutations detected in this study have been deposited in GenBank under the accession numbers EU788003 (K1062M), EU788004 (T1087I), EU788005 (F1174L, TTC/TTA), EU788006 (F1174L, TTC/TTG), EU788007 (F1174C), EU788008 (F1174V), EU788009 (F1245L) and EU788010 (R1275Q). The copy number data as well as the raw microarray data will be accessible from <http://www.ncbi.nlm.nih.gov/geo/> with the accession number GSE12494. Reprints and permissions information is available at www.nature.com/reprints. Correspondence and requests for materials should be addressed to S.O. (sogawa-ty@umin.net) or Y.H. (hayashiy-ty@umin.ac.jp).

METHODS

Specimens. Primary neuroblastoma specimens were obtained during surgery or biopsy from patients who were diagnosed with neuroblastoma and admitted to a number of hospitals in Japan. In total, 215 primary neuroblastoma specimens were subjected to SNP array analysis after informed consent was obtained from the parents of each patient. The patients were staged according to the International Neuroblastoma Staging System²³. The clinicopathological findings are summarized in Supplementary Table 1. Twenty-four neuroblastoma-derived cell lines were also analysed by SNP array analysis (Supplementary Table 2). The SCMC-N2, SCMC-N4 and SCMC-N5 cell lines were established in our laboratory^{24,25}. The SJNB series of cells and the UTP-N-1²⁶ cell line were gifts from A. T. Look and A. Inoue, respectively. The other cell lines used were obtained from the Japanese Cancer Resource Cell Bank (<http://cellbank.nibio.go.jp/>).

Microarray analysis. High molecular mass DNA was isolated from tumour specimens as well as from the peripheral blood or the bone marrow as described previously²⁴. The DNA was subjected to SNP array analysis using Affymetrix GeneChip Mapping 50K and/or 250K arrays (Affymetrix) according to the manufacturer's suggested protocol. The scanned array images were processed with Gene Chip Operation software (GCOS)¹³, followed by SNP calls using GTYE. Genome-wide copy number measurements and loss of heterozygosity detection were performed using CNAG/AsCNAR algorithms¹⁴, which enabled an accurate determination of allele-specific copy numbers.

Confirmation of SNP array data. FISH and/or genomic PCR analysis confirmed the results of SNP array analyses as described previously¹³. PCR primer sets were designed to amplify several adjacent fragments inside and outside of the homozygously deleted regions in tumour samples.

Mutation analysis. Mutations in the *ALK* gene were examined in 239 neuroblastoma samples, including 24 cell lines, by denaturing high-performance liquid chromatography (DHPLC) using the WAVE system (Model 4500; Transgenomic) according to the manufacturer's suggested protocol¹⁶. The samples showing abnormal conformations were subjected to direct sequencing analysis using an ABI PRISM 3100 Genetic Analyser (Applied Biosystems). Using direct sequencing, mutation analysis of *MYCN* was also performed in seven cases with *ALK* alterations but not *MYCN* amplification. The primer sets used in this study are listed in Supplementary Table 5.

Transforming potential of *ALK* mutants. Total RNA was extracted from SJNB-1 (wild type), SCMC-N2 (F1174L) and SCMC-N5 (K1062M) cells as described previously²⁶. First-strand cDNA was synthesized from RNA using Transcriptor Reverse Transcriptase and an oligo (dT) primer (Roche Applied Science). The resulting cDNA was then amplified by PCR using the KOD-Plus-Ver.2 DNA polymerase (Toyobo) and the primers sense 5'-TCAGAAGCTTACCAA-GGACTGTCAGAGC-3' and antisense 5'-AATTGCGCCGCTACTTGTCA-TCGTCCCTTGATGTCGGGCCAGGCTG GTTCATGC-3', thereby introducing a HindIII site at the 5' terminus and a NotI site and a Flag sequence at the 3' terminus. The HindIII-NotI fragments of *ALK* cDNA were subcloned into pcDNA3 to generate expression plasmids. After resequencing to confirm that they had no other mutations, the *ALK* plasmids were used for transfection into NIH3T3 cells using Effectene Transfection Reagent (Qiagen) according to the suggested manufacturer's protocol. The transfected NIH3T3 cells were selected in 800 µg ml⁻¹ G418 for 2 weeks to obtain stably expressing clones.

To evaluate the phosphorylation status of *ALK* mutants, the cell lysates of stable clones were immunoprecipitated with antibodies to Flag (Sigma) and the resulting precipitates were subjected to western blot analysis with the antibody

specific to pTyr 1604 (Cell Signaling Technology) of *ALK* and the generic anti-phosphotyrosine antibody (PY20). The *in vitro* kinase activity of *ALK* mutants was measured using a non-radioactive isotope solid-phase enzyme-linked immunosorbent assay using the Universal Tyrosine Kinase Assay kit (Takara) according to the manufacturer's suggested protocol. We also performed the *in vitro* kinase assay with the synthetic YFF peptide (Operon Biotechnologies) as described previously¹⁸. For anchorage-independent growth analysis, 1 × 10⁵ stably transfected NIH3T3 cells were mixed in 0.3% agarose with 10% FBS-DMEM and plated on 0.6% agarose-coated 35-mm dishes. After culture for 28 days, the colonies of >0.1 mm in diameter were counted. The quantification of the colonies was from three independent experiments. To investigate the downstream signalling of *ALK*, western blot analysis was performed using the anti-ERK1/2, anti-phospho-ERK1/2, anti-AKT, anti-phospho-AKT, anti-STAT3 and anti-phospho-STAT3 antibodies (Cell Signaling Technology)¹⁵.

The cDNA mutant of *ALK* was also inserted into the pMXS plasmid and the constructs were introduced into NIH3T3 cells by the calcium phosphate method as described previously⁹. The cells were then either cultured for 21 days or injected subcutaneously at six sites in three nude mice.

Inhibition of *ALK* through RNAi-mediated knockdown. To suppress the expression of the *ALK* protein, two different pairs of *ALK* siRNAs (*ALK* siRNA1 and *ALK* siRNA2) were obtained (Qiagen)¹⁵. The sequences were 5'-GAGUCUGGCAGUUGACUUCdTdT-3' for *ALK* siRNA1 and 5'-GCUCC-GGGUGCCAAGCAGdTdT-3' for *ALK* siRNA2. A siRNA, targeting a sequence in firefly (*Photinus pyralis*) luciferase mRNA (*luc* siRNA), was used as a negative control (Qiagen)¹⁵. The sequences of *luc* siRNA were as follow: sense 5'-CGUACGCGAAUACUUCGAdTdT-3' and antisense 5'-UCGAAGUAAU-CGCGUACGdTdT-3'. Gene knockdown was achieved in SK-N-SH and LAN-2 cells using HiPerFect transfection reagent following the manufacturer's suggested instructions (Qiagen). To assess the effect of *ALK* knockdown on cell growth, these cells were seeded in 96-well plates at a concentration of 8.0 × 10³ cells per well 24 h before transfection and assayed using the Cell Counting Kit-8 (Wako).

Statistical analysis. The significance of the correlation between *MYCN* amplification and *ALK* mutation was tested according to the conventional 2 × 2 contingency table using Fisher's exact test. The significance of the differences in kinase activity between wild-type and mutant *ALK* kinases was examined by the Mann-Whitney *U*-test based on the measured percentage activity of kinases in the precipitates of the corresponding samples. The significance of the differences in colony formation between wild-type and mutant *ALK* kinases was also examined by the Mann-Whitney *U*-test. The size of the hazards from possible risk factors, including International Neuroblastoma Staging System stages, *MYCN* status and *ALK* mutation/amplification were estimated by Cox regression analysis assuming a proportional hazard model using Stata software. Correlation between ploidy and clinical stage was tested by nptrend test.

23. Smith, E. I., Haase, G. M., Seeger, R. C. & Brodeur, G. M. A surgical perspective on the current staging in neuroblastoma—the International Neuroblastoma Staging System proposal. *J. Pediatr. Surg.* **24**, 386–390 (1989).
24. Takita, J. *et al.* Allelotype of neuroblastoma. *Oncogene* **11**, 1829–1834 (1995).
25. Takita, J. *et al.* Absent or reduced expression of the caspase 8 gene occurs frequently in neuroblastoma, but not commonly in Ewing sarcoma or rhabdomyosarcoma. *Med. Pediatr. Oncol.* **35**, 541–543 (2000).
26. Takita, J. *et al.* Allelic imbalance on chromosome 2q and alterations of the caspase 8 gene in neuroblastoma. *Oncogene* **20**, 4424–4432 (2001).

Chromosome copy number analysis in screening for prognosis-related genomic regions in colorectal carcinoma

Kentaro Kurashina,^{1,2} Yoshihiro Yamashita,¹ Toshihide Ueno,¹ Koji Koinuma,² Jun Ohashi,³ Hisanaga Horie,² Yasuyuki Miyakura,² Toru Hamada,^{1,2} Hidenori Haruta,^{1,2} Hisashi Hatanaka,¹ Manabu Soda,¹ Young Lim Choi,¹ Shuji Takada,¹ Yoshikazu Yasuda,² Hideo Nagai² and Hiroyuki Mano^{1,4,5}

¹Division of Functional Genomics and ²Department of Surgery, Jichi Medical University, Tochigi 329-0498; ³Department of Human Genetics, Graduate School of Medicine, University of Tokyo, Tokyo 113-0033; ⁴CREST (Core Research for Evolutional Science and Technology), Japan Science and Technology Agency, Saitama 332-0012, Japan

(Received March 9, 2008/Revised May 12, 2008/Accepted May 13, 2008/Online publication June 28, 2008)

Colorectal carcinoma (CRC) remains the major cause of cancer death in humans. Although chromosomal structural anomaly is presumed to play an important role in the carcinogenesis of CRC, chromosomal copy number alterations (CNA) and loss of heterozygosity (LOH) have not yet been analyzed extensively at high resolution in CRC. Here we aim to identify recurrent CNA and LOH in human CRC with the use of single nucleotide polymorphism-typing microarrays, and to reveal their relevance to clinical outcome. Surgically resected CRC specimens and paired normal mucosa were obtained from a consecutive series of 94 patients with CRC, and both of them were subjected to genotyping with Affymetrix Mapping 50K arrays. CNA and LOH were inferred computationally on every single nucleotide polymorphism site by integrating the array data for paired specimens. Our large dataset reveals recurrent CNA in CRC at chromosomes 7, 8, 13, 18, and 20, and recurrent LOH at chromosomes 1p, 4q, 5q, 8p, 11q, 14q, 15q, 17p, 18, and 22. Frequent uniparental disomy was also identified in chromosomes 8p, 17p, and 18q. Very common CNA and LOH were present at narrow loci of <1 Mbp containing only a few genes. In addition, we revealed a number of novel CNA and LOH that were linked statistically to the prognosis of the patients. The precise and large-scale measurement of CNA and LOH in the CRC genome is efficient for pinpointing prognosis-related genome regions as well as providing a list of unknown genes that are likely to be involved in CRC development. (*Cancer Sci* 2008; 99: 1835–1840)

Colorectal carcinoma (CRC) remains the fourth most prevalent cancer and the second highest cause of cancer death in the USA.⁽¹⁾ The life expectancy of individuals with CRC is mainly dependent on the clinical stage when CRC is detected, and the current chemotherapeutic regimens can only marginally improve the prognosis of advanced cases.⁽²⁾ To achieve better outcomes for such individuals, it would be desirable to identify and target cellular molecules involved in the carcinogenesis of CRC.

A variety of genetic alterations take place, in a defined order, during the development of CRC.⁽³⁾ In addition to nucleotide sequence mutations and epigenetic abnormalities of genes, structural changes of chromosomes and chromosomal instability (CIN) are known to play a major role in the carcinogenesis of CRC.⁽⁴⁾ Gene amplification may induce oncogenic activity in a subset of protooncogenes, such as *MYC*, *MYCN*, *ERBB2*, and *CCND1*. In contrast, deletion or truncation of tumor-suppressor genes may confer inactivation of their function. These chromosomal copy number alterations (CNA) can be as large as numerical anomaly of entire chromosomes, or as small as segmental amplification or deletion of <10 kb.

Further, loss of heterozygosity (LOH) of the genome is frequently present in cancer cells, where one allele of a chromosome is

deleted (chromosome copy number of one) or the remaining allele is further duplicated (chromosome copy number of two), referred to as uniparental disomy (UPD). It has been hypothesized that such regions likely harbor mutated or epigenetically silenced tumor-suppressor genes. However, recent evidence indicates that these regions may also carry activated oncogenes, as demonstrated for mutated *JAK2* in myeloproliferative disorders.⁽⁵⁾

In addition to the conventional array-based comparative genomic hybridization (CGH) technique,^(6,7) microarrays developed originally for single nucleotide polymorphism (SNP) typing are now being applied to CIN investigation.^(8–10) The main advantage of the latter system over the former is that it readily screens CIN at very high resolution in an allele-specific manner. The SNP arrays are thus able to screen for both CNA and LOH throughout the genome.

A few studies have been conducted recently for the SNP array-based CIN analysis of CRC,^(11–14) but the interpretation of such data may be hampered by the small number of clinical specimens and the lack of paired normal samples for the analysis (especially in the cases of LOH examination).

Here we have collected CRC and paired normal specimens from a total of 94 individuals with CRC, and hybridized each DNA to Affymetrix Mapping 50K Xba 240 microarrays (Affymetrix, Santa Clara, CA, USA), which are able to examine CNA and LOH at a mean resolution of 47.2 kb. Application of bioinformatics to these large datasets has identified a number of novel prognosis-related regions in the CRC genome.

Materials and Methods

Preparation of genomic DNA. Primary tumors and paired colonic mucosal specimens (as normal controls) were surgically resected and frozen from a total of 94 individuals with sporadic CRC (from January 2002 to March 2003 at Jichi Medical University Hospital). The clinical characteristics of these study subjects are summarized in Suppl. Table S1. Informed consent was obtained from each subject according to the protocols approved by the ethics committees of Jichi Medical University. Genomic DNA was extracted from the samples with the use of the QIAamp DNA Mini Kit (Qiagen, Valencia, CA, USA) according to manufacturer's instructions. The microsatellite instability (MSI) status of each tumor was determined on the basis of the analysis of nine microsatellite repeat loci as described previously.⁽¹⁵⁾

⁵To whom correspondence should be addressed. E-mail: hmano@jichi.ac.jp

Hybridization with SNP-typing arrays. Each DNA sample (250 ng) was digested with *Xba*I, ligated to Adaptor-Xba (Affymetrix), amplified by polymerase chain reaction (PCR), and subjected to hybridization with Mapping 50K Xba 240 arrays (Affymetrix). SNP genotyping calls were generated using GDAS software version 3.0 (Affymetrix) with a confidence score threshold of 0.05. Chromosome copy number and allele-specific copy number at each SNP site were calculated from the hybridization signal intensity for both CRC and paired normal mucosa specimens with the use of CNAG software (<http://www.genome.umin.jp>).⁽⁸⁾ Only the CNAG data for autosomes were analyzed in the present study. Genotype-call data and original CEL files are available at the Gene Expression Omnibus website (<http://www.ncbi.nlm.nih.gov/geo>) under the accession number GSE11417, and CNAG output data are available upon request. We considered chromosome copy number changes or LOH data reliable only when contiguous SNP probes presented the same data.

Quantitative real-time PCR. RNA was isolated from the samples with the use of an RNeasy Mini column (Qiagen) and was used to synthesize cDNA with PowerScript reverse transcriptase (Clontech, Palo Alto, CA, USA). Portions of genomic DNA or cDNA were subjected to PCR with the QuantiTect SYBR Green PCR Kit (Qiagen). The amplification protocol comprised incubations at 94°C for 15 s, 60°C for 30 s, and 72°C for 60 s. Incorporation of the SYBR Green dye into the PCR products was monitored in real time with the ABI PRISM 7700 sequence detection system (Applied Biosystems, Foster City, CA, USA), thereby allowing determination of the threshold cycle (C_T) at which exponential amplification of products begins. To quantitate the genomic DNA, the C_T values for genomic DNA corresponding to the glyceraldehyde-3-phosphate dehydrogenase (*GAPDH*) gene and the target regions were used to calculate the abundance of target regions relative to that of *GAPDH* DNA. The primer sequences used for PCR were: 5'-AGGACATTTGTAATCAGTATCTGTG-3' and 5'-AGGGCAGTCAATAAGCTAAGGAA-3' for period homolog 3 (*PER3*); 5'-CTCAACTTCCTTGAGCACCCTCTG-3' and 5'-TACCTTGGACAGCTTGCTCTGTTG-3' for invasion inhibitory protein 45 (*IIP45*); 5'-ACTGGTGCTCTCACTGTCCAAAAC-3' and 5'-CGCAGAGTAGACATCCTGGGTAAA-3' for FAT tumor suppressor homolog (*FAT*); 5'-AGCGAATGGAAGTAAATTTGG-3' and 5'-TGCATCTGTCCTAATCTACTCT-3' for breast cancer cell 2 (*BRCC2*); 5'-AGAGACTGTATTGCAGGGTGAAGA-3' and 5'-CTTCCATTATATGTCCCGACTCC-3' for v-maf musculoaponeurotic fibrosarcoma oncogene homolog K (*MAFK*); 5'-CTACTCTCTTGCCAGCATTTCAC-3' and 5'-ACCTAAGCCTTATCCACACCTCAC-3' for protein tyrosine phosphatase, non-receptor type 1 (*PTPNI*); 5'-GTCATAGCCCTGCCTTCT-3' and 5'-GGTCCCCAAAACGCACACTC-3' for *CSMD1*; and 5'-CTGACCTGCCGCTCTAGAAAACCT-3' and 5'-CAGGAAATGAGCTTGACAAAAGTGG-3' for *GAPDH*.

Similarly, the relative quantity of cDNA was calculated using the C_T value of PCR for each cDNA and that for the *GAPDH* cDNA. The primer sequences for reverse transcription (RT)-PCR were: 5'-CGGTTTTCTACAACACATTAGCA-3' and 5'-ACTGGAAGGTGGGAAATCAATAGG-3' for *PER3* cDNA; 5'-CTGGAACCTCAGGCAGCAGACAAG-3' and 5'-GACTCCTGGGGGAGAACAGCATT-3' for *IIP45* cDNA; 5'-GTGAGTAATCCGCGCTGTTCTTT-3' and 5'-CAGTAGTTGGGACACTGGAAATGG-3' for *FAT* cDNA; 5'-GACAGATTCGCCCAT-TATTAGG-3' and 5'-TGTTTCTCTGCACAATTTGAACCA-3' for *BRCC2* cDNA; 5'-GCCATATACCACTCTCCCTTCCAC-3' and 5'-TGGAGTGTGCCTTGATTCATACA-3' for *CSMD1*; and 5'-GTCAGTGGTGGACCTGACCT-3' and 5'-TGAGCTTGACAAAGTGGTCG-3' for *GAPDH* cDNA. The primer sets for *MAFK* and *PTPNI* cDNA were the same ones used for genomic amplification of the corresponding genes.

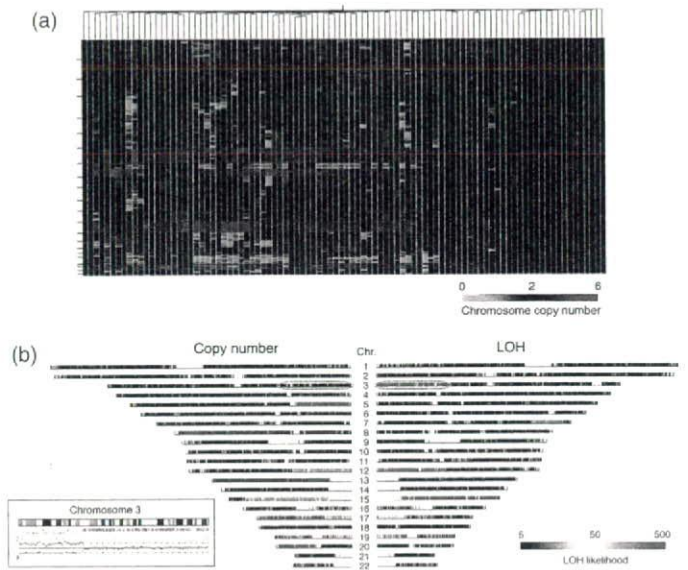


Fig. 1. Chromosomal copy number alterations and loss of heterozygosity (LOH) in the colorectal carcinoma genome. (a) The study subjects ($n = 94$) were subjected to a hierarchical clustering analysis based on the inferred copy number for all autosomal single nucleotide polymorphism (SNP) sites. Copy number is color coded according to the indicated scheme at the bottom. SNP sites are ordered by their physical position from top to bottom, and the borders between chromosomes are indicated by small bars at the left. (b) Chromosome copy number (left panel) and LOH likelihood score (right panel) are demonstrated for patient ID#002 in a chromosome view in a symmetrical manner. Copy number value is color coded as in (a), and LOH likelihood score is colored according to the scheme indicated at the bottom. Chromosome numbers are shown at the center. The allele-specific copy number data for the 3p region (indicated by a blue circle) is demonstrated in the inset as pink and green lines. Below the cytoband figure, the positions of SNP sites with a hetero- or discordant-call are indicated by green or pink bars, respectively.

Statistical analysis. Hierarchical clustering of the dataset and Student's *t*-test were carried out using GeneSpring 7.0 software (Agilent Technologies, Santa Clara, CA, USA), and survival analyses were carried out with SAS software (version 8.0.2: SAS Inc., Cary, NC, US) and the 'Survival' package in R version 2.6.0 (<http://www.R-project.org>). The *q*-values for the false discovery rate were calculated directly from the ordered *P*-values above using the 'Q-value' software (<http://genomics.princeton.edu/storeylab/qvalue/>) developed by Storey *et al.*⁽¹⁶⁾ with parameters defined by Jones *et al.*⁽¹⁷⁾

Results

Frequent CAN. Genomic DNA was extracted from both CRC specimens and normal mucosa obtained from the same study subjects ($n = 94$). Both data were integrated into the CNAG software to infer chromosome copy number at every SNP site for each CRC sample. Incorporation of the data for paired normal mucosa markedly increased the accuracy of the calculation; the mean probe-signal intensity at diploid chromosomes in CRC was inferred from the data of control samples (where the majority of the chromosomes were expected to be diploid). Chromosome copy number data at each SNP probe site ($n = 57\,290$ for all autosomal SNP) was thus calculated for all CRC specimens, and a hierarchical clustering analysis for the study subjects was conducted based on the overall CNA profile. As shown in Figure 1a and Suppl. Fig. S1, approximately one-quarter of the subjects (the right side branch in the figure) had stable chromosomes, but the remaining samples had

Table 1. Frequent regions of chromosomal copy number alterations or loss of heterozygosity (LOH) in colorectal carcinoma patients

| Change | Chromosome | Nucleotide position | Mapped RefSeq gene | GenBank accession no. |
|---|------------|-------------------------|--------------------|-----------------------|
| Gain (chromosome copy no. ≥ 5 in ≥ 15 subjects) | | | | |
| | 6 | 16,176,003–16,176,549 | None | |
| | 8 | 70,887,465–71,089,425 | <i>SLCO5A1</i> | NM_030958.1 |
| | 20 | 31,768,314–31,919,527 | <i>PXMP4</i> | NM_007238.4 |
| | | | <i>ZNF341</i> | NM_032819.3 |
| | | | <i>CHMP4B</i> | NM_176812.3 |
| Decrease (chromosome copy no. ≤ 1 in ≥ 35 subjects) | | | | |
| | 18 | 60,114,744–61,522,755 | None | |
| | 18 | 64,600,350–65,380,261 | <i>CCDC102B</i> | NM_024781.1 |
| | | | <i>DOK6</i> | NM_152721.2 |
| | 18 | 67,791,010–68,366,009 | <i>CBLN2</i> | NM_182511.2 |
| Homozygous deletion (common in two subjects) | | | | |
| | 3 | 60,393,402–60,490,818 | <i>FHIT</i> | NM_002012.1 |
| | 20 | 14,796,659–15,040,864 | <i>C20orf133</i> | NM_080676.5 |
| LOH (common in ≥ 55 subjects) | | | | |
| | 5 | 108,765,615–112,484,272 | <i>APC</i> | NM_000038.3 |
| | 17 | 5,265,130–8,883,455 | <i>TP53</i> | NM_000546.3 |
| | | | <i>XAF1</i> | NM_017523.2 |
| | | | <i>DVL2</i> | NM_004422.2 |
| | 17 | 11,076,427–12,490,201 | Others | |

frequent CNA of various sizes. For instance, gross amplification was found commonly in chromosomes 7, 8q, 13, and 20, whereas large deletions of chromosomes were identified in 8p and 18.

Further, in-depth analysis of the dataset identified amplifications of various magnitudes at various frequencies. For instance, a high-grade amplification of the genome (copy number of five or greater) was found at three different loci in the genome of ≥ 15 subjects (Table 1), the size of which ranged from 547 to 201 961 bp. Surprisingly, amplification of one of these loci at chromosome 8q was found among as many as 25 patients (the most common, highly amplified region in our dataset). As expected, low-grade amplifications of the genome were found more commonly; a region of ~ 2.7 Mbp at chromosome 20q was, for example, amplified to four or more copies in more than 30 subjects, and this grade of amplification was also identified at many loci throughout the genome. For instance, genome regions with a copy number of four or greater in $\geq 10\%$ of the patients were mapped to chromosomes 7p, 8q, 13, 20q, and others, comprising a total of 1921 SNP sites (3.4% of all sites).

Similarly, a decrease in chromosome copy number ($n \leq 1$) was also frequently identified throughout the genome; three distinct loci had such decreases in ≥ 35 subjects (Table 1). Further, a less-frequent decrease (found in $\geq 10\%$ of patients) was mapped to chromosomes 1p, 5q, 8p, 14q, 17p, and others, comprising 3899 SNP sites in total (6.8% of all sites).

In our dataset, common homozygous deletions were unexpectedly rare. Only two loci demonstrated a chromosome copy number of zero in two individuals (Table 1). Interestingly, one such loci on chromosome 3 is known to be a common fragile region containing the fragile histidine triad gene (*FHIT*, GenBank accession no. NM_002012.1), a putative tumor suppressor.⁽¹⁸⁾ The other homozygous deletion site at chromosome 20 spans 244 206 bp containing only one unknown gene, *C20orf133* (GenBank accession no. NM_080676.5).

Frequent LOH. With the SNP-typing array platform, we can carry out SNP genotyping by comparing the signal intensity between two alleles, which reflects the DNA amount of each allele. In the present study, with a moving window for 21 contiguous SNP, allele-specific copy number decreases were examined to identify LOH regions. Three most common LOH loci (found in 55 cases) were thus mapped to chromosomes

5 and 17 (Table 1). Other frequent LOH (found in $\geq 20\%$ of patients) were identified on chromosomes 1p, 4q, 5q, 8p, 11q, 14q, 15q, 17p, 18, and 22. Less-frequent LOH were seen in two large loci (chromosomes 10 and 16), which contain a tumor necrosis factor receptor superfamily member (*FAS*, GenBank accession no. NM_000043.3) and ataxin-2 binding protein 1 (*A2BP1*, GenBank accession no. NM_018723.2).

Genome regions with UPD may contain tumor-suppressor genes (where both alleles carry a mutated, inactivated tumor-suppressor gene) or oncogenes (where cancer cells have two copies of a mutated and activated oncogene). CRC may have UPD at specific loci as demonstrated by Andersen *et al.*⁽¹⁹⁾ In our dataset, we readily identified UPD regions that were characterized by a chromosome copy number of two and an LOH likelihood score of ≥ 50 defined by the CNAG software. In the data for patient ID# 002, for instance, a very high LOH likelihood score was inferred on chromosomes 3p and 15q (right panel of Fig. 1b). Although the latter region of the genome had a decreased copy number (left panel), the former was supposed to be diploid, indicating the presence of UPD. SNP array-based analysis can measure in detail changes in copy number in an allele-specific manner. With such analysis, as shown in the inset in Figure 1b, one allele at 3p was indeed amplified to a copy number of two (pink line), but the other allele was deleted (green line) in the same region, thus confirming the presence of UPD. Similar UPD was also identified on chromosomes 5q, 8p, 11, 14, 15, 17p, and 18q in our dataset.

Verification of the CNA data. The inferred copy number of chromosomes was then verified by quantitative real-time PCR. First, four genes (*BRCC2*, GenBank accession no. NM_001001786.1; *FAT*, GenBank accession no. NM_005245.3; *IIP45*, GenBank accession no. NM_021933.2; and *PER3*, GenBank accession no. NM_016831.1) mapped to independent loci with a frequent copy number loss were chosen to measure DNA quantity. The amount of DNA of each gene relative to that of *GAPDH* was examined in the patients with an inferred copy number of two and those with a copy number of one. As shown in the left panel of Figure 2a, the relative DNA amount of each gene was decreased to 0.7–0.5 in the patients with the copy number loss; 0.65 ± 0.52 (mean \pm SD), 0.56 ± 0.26 , 0.65 ± 0.22 , and 0.73 ± 0.33 for *BRCC2*, *FAT*, *IIP45*, and *PER3*, respectively. The correlation coefficients between inferred copy number by

Table 2. Prognosis-related regions of copy number alterations (CNA) or loss of heterozygosity (LOH) in colorectal carcinoma patients

| Change | Chromosome | Position | Size (Mbp) | P-value | q-value | Mapped RefSeq gene | GenBank accession no. |
|--------|------------|-------------------------|------------|---------|-------------|--------------------------|------------------------|
| CNA | 5 | 113,733,368–117,078,267 | 3.34 | <0.001 | 0.095 | <i>SEMA6A</i> and others | NM_20796.3 and others |
| | 5 | 121,427,436–122,773,632 | 1.35 | <0.001 | 0.095 | <i>LOX</i> and others | NM_002317.3 and others |
| | 5 | 123,233,993–126,057,451 | 2.82 | <0.0005 | 0.095 | Others | |
| | 5 | 142,509,574–142,681,049 | 0.17 | <0.001 | 0.095 | Others | |
| | 5 | 160,137,590–160,786,796 | 0.65 | <0.001 | 0.098 | Others | |
| | 5 | 162,659,919–162,863,325 | 0.20 | <0.0005 | 0.095 | <i>CCNG1</i> and others | NM_004060.3 and others |
| | 6 | 109,126,299–109,435,125 | 0.31 | <0.0005 | 0.095 | <i>SESN1</i> and others | NM_014454.1 and others |
| | 10 | 110,674,541–111,338,259 | 0.66 | <0.0005 | 0.095 | None | |
| | 18 | 51,345,876–52,332,836 | 0.99 | <0.0005 | 0.095 | <i>TCF4</i> and others | NM_003199.2 and others |
| | 18 | 53,401,262–55,536,937 | 2.14 | <0.0005 | 0.095 | <i>RAX</i> and others | NM_013435.2 and others |
| LOH | 16 | 4,858,366–6,679,934 | 1.82 | <0.0001 | 0.046–0.224 | <i>UBN1</i> and others | NM_002705.4 and others |
| | 16 | 7,010,644–7,608,397 | 0.60 | <0.0005 | 0.181 | <i>AZBP1</i> | NM_018723.2 |

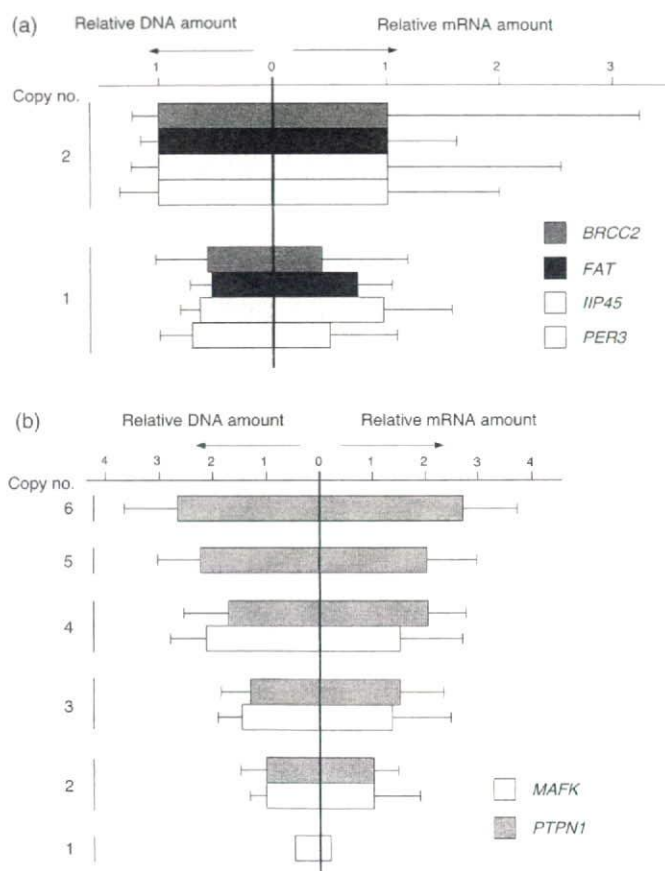


Fig. 2. Verification of copy number changes. (a) The DNA quantities of *PER3*, *IIP34*, *FAT*, and *BRCC2* (relative to that of *GAPDH*) were measured by real-time polymerase chain reaction in the subjects with inferred copy number two ($n = 2$) or one ($n = 1$). The mean + SD value for each gene was normalized to the corresponding mean value for the group with diploid chromosomes, and is shown in the left panel. The mRNA amount for each gene (relative to that of *GAPDH*) was also quantitated by real-time reverse transcription-polymerase chain reaction and is shown in a similar way. (b) The relative DNA (left panel) or mRNA (right panel) of *MAFK* and *PTPN1* was calculated as in (a).

array hybridization and DNA quantification by PCR were 0.219, 0.383, 0.216, and 0.314, respectively.

For the same gene set, we also examined how copy number changes affect mRNA level. Quantitative real-time reverse transcription-PCR was used to quantify the relative amount of

each mRNA to that of *GAPDH* (right panel of Fig. 2a). Similar to the chromosome copy number, the mean mRNA level in the samples with copy number loss was decreased compared to the level in those without the loss; 0.47 ± 0.75 , 0.80 ± 0.29 , 0.97 ± 0.64 , and 0.54 ± 0.69 for *BRCC2*, *FAT*, *IIP45*, and *PER3*, respectively. However, a relatively large SD in each mRNA amount indicates that transcriptional level was also influenced significantly by other factors such as epigenetic regulation and transcriptional factors.

We also measured the DNA amount of two genes (*MAFK*, GenBank accession no. NM_002360.3, and *PTPN1*, GenBank accession no. NM_002827.2) that showed various levels of copy number amplification in our dataset. As shown in the left panel of Figure 2b, the calculated DNA amount of *MAFK* relative to that of *GAPDH* by quantitative PCR paralleled the copy number inferred from SNP arrays. Similarly, DNA quantity measured by real-time PCR for *PTPN1* generally followed the inferred copy number ($n = 2-6$). Again, the mRNA from each gene was quantified by real-time reverse transcription-PCR, revealing that amount of DNA significantly affects mRNA level (right panel).

Prognosis-related CNA and LOH. To directly search for CNA and LOH linked to the survival of patients, we utilized Cox's proportional-hazard regression analysis⁽²⁰⁾ coupled with the false-discovery rate correction on the copy number profile of all autosomal SNP sites.

From the CNA dataset, several loci at chromosomes 5, 6, 10, and 18 were proved to be significantly related to prognosis ($P < 0.001$ and $q < 0.1$) (Table 2). For all loci except one at chromosome 10, chromosomal loss had a negative impact on the outcome of the patients (Fig. 3a). One locus at chromosome 5 contains the cyclin G1 gene (*CCNG1*, GenBank accession no. NM_004060), which belongs to the cyclin gene superfamily. In contrast to the other cyclins, expression of *CCNG1* is stable throughout the cell cycle, and becomes activated in mouse cells by exposure to ionizing radiation, which also induces cell cycle arrest.⁽²¹⁾ Further, disruption of WT1 function is linked to the downregulation of *CCNG1* expression.⁽²²⁾ These data together indicate a pro-apoptotic role for *CCNG1*, and our discovery of a relationship between loss of *CCNG1* and poor prognosis may imply a function of *CCNG1* as a tumor suppressor in CRC.

In addition to CNA analysis, we further searched for prognosis-related LOH with the following approach. There were many recurrent LOH regions in our dataset at various frequencies. We thus examined whether some of those recurrent alterations (observed in five or more samples) were preferentially present in the patients who died of CRC compared to those who survived in our observation period. For these potentially outcome-related genomic regions, prognosis was compared statistically between the two subject groups by the log-rank test with the false-discovery

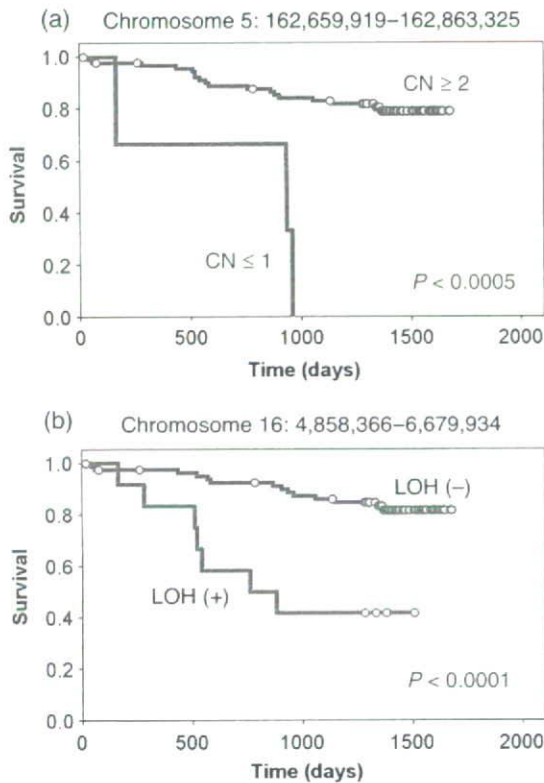


Fig. 3. Prognosis-related copy number (CN) loss and loss of heterozygosity (LOH). The survival of the subjects with or without copy number loss of a locus at (a) chromosome 5 or (b) chromosome 16 was compared using Kaplan-Meier analysis. The *P*-value for each comparison was calculated using the log rank test.

rate correction. We finally isolated two loci of LOH where the presence of LOH was related to a short survival time ($P < 0.0005$) (Table 2; Fig. 3b). One such prognosis-related LOH locus contains the ubinuclein 1 gene (*UBN1*, GenBank accession no. NM_016936). Because *UBN1* associates physically with *API1* and interferes with its DNA-binding activity,⁽²³⁾ *UBN1* may also function to suppress tumor development.

Discussion

We have here calculated chromosome copy number as well as LOH likelihood throughout the genome of 94 CRC specimens. Together with the clinical information for the study subjects, we identified many loci whose DNA quantity or LOH is associated with the survival and various characteristics of CRC subjects. Some of the RefSeq genes mapped on such loci are well-known cancer-related genes. One frequent LOH was mapped to a genomic region of approximately 235 kb only containing the *MCC* gene, which had already been shown to be prone to somatic mutations and deletions in CRC and other cancers.^(24,25) Overexpression of *MCC* suppresses the G_1 to S transition of the cell cycle, whereas such activity is lost for an *MCC* mutant identified in CRC,⁽²⁶⁾ supporting the tumor-suppressor activity of *MCC*.

In addition to the analysis presented in the present manuscript, our large dataset can also be utilized to characterize other aspects of CRC. CRC may be subdivided into microsatellite-stable

cancer and MSI-high cancer. Comparison of our copy number data between the two subgroups has identified a locus of only 56 kb long, the copy number of which was statistically different between the subgroups ($P < 0.001$). This region contains only one RefSeq gene, ribosomal protein S6 kinase 90-kDa 5 (*RPS6KA5*, GenBank accession no. NM_004755.2), discovering another unexpected linkage between MSI and mitogen-activated protein kinase (MAPK) functions. A similar comparison of our data between the CRC with or without lymph node metastasis has identified two distinct loci in the genome (Suppl. Table S2). Also, a narrow genomic region was identified, the LOH of which is linked to the presence of liver metastasis ($P < 0.001$). However, that locus does not contain any RefSeq genes. Given the high resolution of SNP-typing arrays for CNA and LOH analysis, many genomic regions identified in this manuscript are <100 kb and contain only a few RefSeq genes per locus (Tables 1,2). Thus, our analysis is highly useful in narrowing down the list of genes associated with various characteristics of CRC.

Copy number alterations of CRC specimens have been studied with bacterial artificial chromosome array-based CGH,^(13,27,28) and large segmental changes of chromosomes in such reports and publicly available databases match well with those identified in our study (see, for example, <http://www.cgtdm.jp/CGHDatabase/tumor?lang=en>). Although SNP-typing array-based CNA and LOH analyses have been reported recently for CRC, information for genes involved directly in such CNA and LOH is scarce.⁽¹¹⁻¹⁴⁾ Lips *et al.* examined the LOH status of paraffin-embedded CRC specimens ($n = 4$) and found recurrent LOH at chromosomes 5q, 17p, 18, and 20,^(13,14) the former three of which were indeed identified in our study. However, Gaasenbeek identified LOH at the *TP53* locus in MSI-positive CRC.⁽¹³⁾ In our cohort, however, there was only one MSI-positive case among 55 cases with LOH at *TP53*, whereas four were positive for MSI among 39 individuals without LOH at the locus, indicating no significant linkage between MSI and LOH at *TP53* (Fisher's exact test, $P = 0.186$).

It should, however, be noted that the RefSeq genes may not be the sole players in carcinogenesis. Long non-coding RNA is known to be involved in methylation of the genome,⁽²⁹⁾ and short non-coding RNA such as microRNA may be involved directly in cell growth and differentiation.⁽³⁰⁾ These transcripts, despite their inability to synthesize proteins, may thus contribute to the characteristics of CRC. As the discovery and annotation of these non-coding RNAs is still in its infancy,^(31,32) many loci identified through our analysis may contain yet-undiscovered non-coding RNA, and these transcripts, not protein-coding mRNA, may play an important role in carcinogenesis as well. Indeed, one of the loci linked to lymph node metastasis has no RefSeq genes but only one non-coding RNA (Suppl. Table S2).

Our analysis provides a large-scale, accurate CNA and LOH dataset together with detailed information of clinical characteristics (including survival information in Suppl. Table S1) for the subjects. These data may become a framework for further analysis on structural alterations of the cancer genome in CRC.

Acknowledgments

The present study was supported in part by a Grant-in-Aid for Third-Term Comprehensive Control Research for Cancer from the Ministry of Health, Labor, and Welfare of Japan, and by a grant for 'High-Tech Research Center' Project for Private Universities: Matching Fund Subsidy, from the Ministry of Education, Culture, Sports, Science, and Technology of Japan (2002-06) to HM.

References

- Jemal A, Siegel R, Ward E *et al.* Cancer statistics, 2006. *CA Cancer J Clin* 2006; **56**: 106-30.

- Portier G, Elias D, Bouche O *et al.* Multicenter randomized trial of adjuvant fluorouracil and folinic acid compared with surgery alone after resection of colorectal liver metastases: FFD ACHBTH AURC 9002 trial. *J Clin Oncol* 2006; **24**: 4976-82.

- 3 Fearon ER, Vogelstein B. A genetic model for colorectal tumorigenesis. *Cell* 1990; **61**: 759–67.
- 4 Lengauer C, Kinzler KW, Vogelstein B. Genetic instabilities in human cancers. *Nature* 1998; **396**: 643–9.
- 5 Kralovics R, Passamonti F, Buser AS *et al*. A gain-of-function mutation of JAK2 in myeloproliferative disorders. *N Engl J Med* 2005; **352**: 1779–90.
- 6 Jiang JK, Chen YJ, Lin CH, Yu IT, Lin JK. Genetic changes and clonality relationship between primary colorectal cancers and their pulmonary metastases – an analysis by comparative genomic hybridization. *Genes Chromosomes Cancer* 2005; **43**: 25–36.
- 7 Kleivi K, Teixeira MR, Eknaes M *et al*. Genome signatures of colon carcinoma cell lines. *Cancer Genet Cytogenet* 2004; **155**: 119–31.
- 8 Nannya Y, Sanada M, Nakazaki K *et al*. A robust algorithm for copy number detection using high-density oligonucleotide single nucleotide polymorphism genotyping arrays. *Cancer Res* 2005; **65**: 6071–9.
- 9 Lin M, Wei LJ, Sellers WR, Lieberfarb M, Wong WH, Li C. dChipSNP: significance curve and clustering of SNP-array-based loss-of-heterozygosity data. *Bioinformatics* 2004; **20**: 1233–40.
- 10 Redon R, Ishikawa S, Fitch KR *et al*. Global variation in copy number in the human genome. *Nature* 2006; **444**: 444–54.
- 11 Andersen CL, Wiuf C, Kruhoffer M, Korsgaard M, Laurberg S, Orntoft TF. Frequent occurrence of uniparental disomy in colorectal cancer. *Carcinogenesis* 2007; **28**: 38–48.
- 12 Tsafirir D, Bacolod M, Selvanayagam Z *et al*. Relationship of gene expression and chromosomal abnormalities in colorectal cancer. *Cancer Res* 2006; **66**: 2129–37.
- 13 Gaasenbeek M, Howarth K, Rowan AJ *et al*. Combined array-comparative genomic hybridization and single-nucleotide polymorphism-loss of heterozygosity analysis reveals complex changes and multiple forms of chromosomal instability in colorectal cancers. *Cancer Res* 2006; **66**: 3471–9.
- 14 Lips EH, Dierssen JW, van Eijk R *et al*. Reliable high-throughput genotyping and loss-of-heterozygosity detection in formalin-fixed, paraffin-embedded tumors using single nucleotide polymorphism arrays. *Cancer Res* 2005; **65**: 10 188–91.
- 15 Miyakura Y, Sugano K, Konishi F *et al*. Extensive methylation of *hMLH1* promoter region predominates in proximal colon cancer with microsatellite instability. *Gastroenterology* 2001; **121**: 1300–9.
- 16 Storey JD, Tibshirani R. Statistical significance for genomewide studies. *Proc Natl Acad Sci USA* 2003; **100**: 9440–5.
- 17 Jones HE, Ohlssen DI, Spiegelhalter DJ. Use of the false discovery rate when comparing multiple health care providers. *J Clin Epidemiol* 2008; **61**: 232–40.
- 18 Zanasi N, Fidanza V, Fong LY *et al*. The tumor spectrum in FHIT-deficient mice. *Proc Natl Acad Sci USA* 2001; **98**: 10 250–5.
- 19 Andersen CL, Wiuf C, Kruhoffer M, Korsgaard M, Laurberg S, Orntoft TF. Frequent occurrence of uniparental disomy in colorectal cancer. *Carcinogenesis* 2006; **28**: 38–48.
- 20 Cox DR. Regression models and life tables. *J R Stat Soc* 1972; **34**: 187–220.
- 21 Sugihara T, Magae J, Wadhwa R *et al*. Dose and dose-rate effects of low-dose ionizing radiation on activation of Trp53 in immortalized murine cells. *Radiat Res* 2004; **162**: 296–307.
- 22 Wagner KJ, Patek CE, Miles C, Christie S, Brookes AJ, Hooper ML. Truncation of WT1 results in downregulation of cyclin G1 and IGFBP-4 expression. *Biochem Biophys Res Commun* 2001; **287**: 977–82.
- 23 Aho S, Buisson M, Pajunen T *et al*. Ubinuclein, a novel nuclear protein interacting with cellular and viral transcription factors. *J Cell Biol* 2000; **148**: 1165–76.
- 24 Kinzler KW, Nilbert MC, Vogelstein B *et al*. Identification of a gene located at chromosome 5q21 that is mutated in colorectal cancers. *Science* 1991; **251**: 1366–70.
- 25 Cawkwell L, Lewis FA, Quirke P. Frequency of allele loss of DCC, p53, RBI, WT1, NF1, NM23 and APC/MCC in colorectal cancer assayed by fluorescent multiplex polymerase chain reaction. *Br J Cancer* 1994; **70**: 813–18.
- 26 Matsumine A, Senda T, Baeg GH *et al*. MCC, a cytoplasmic protein that blocks cell cycle progression from the G₀/G₁ to S phase. *J Biol Chem* 1996; **271**: 10 341–6.
- 27 Fijneman RJ, Carvalho B, Postma C, Mongera S, van Hinsbergh VW, Meijer GA. Loss of 1p36, gain of 8q24, and loss of 9q34 are associated with stroma percentage of colorectal cancer. *Cancer Lett* 2007; **258**: 223–9.
- 28 Jones AM, Douglas EJ, Halford SE *et al*. Array-CGH analysis of microsatellite-stable, near-diploid bowel cancers and comparison with other types of colorectal carcinoma. *Oncogene* 2005; **24**: 118–29.
- 29 Chang SC, Tucker T, Thorogood NP, Brown CJ. Mechanisms of X-chromosome inactivation. *Front Biosci* 2006; **11**: 852–66.
- 30 Carrington JC, Ambros V. Role of microRNAs in plant and animal development. *Science* 2003; **301**: 336–8.
- 31 Carninci P, Kasukawa T, Katayama S *et al*. The transcriptional landscape of the mammalian genome. *Science* 2005; **309**: 1559–63.
- 32 Takada S, Berezikov E, Yamashita Y *et al*. Mouse microRNA profiles determined with a new and sensitive cloning method. *Nucleic Acids Res* 2006; **34**: e115.

Supporting Information

Additional Supporting Information may be found in the online version of this article:

Fig. S1. Hierarchical clustering tree in Figure 1a is demonstrated with subject ID indicated at the bottom.

Table S1. Clinical characteristics of the study subjects

Table S2. Chromosomal copy number alterations (CNA) and loss of heterozygosity (LOH) related to clinical characteristics of colorectal carcinoma

Please note: Blackwell Publishing are not responsible for the content or functionality of any supporting materials supplied by the authors. Any queries (other than missing material) should be directed to the corresponding author for the article.

Identification of Novel Isoforms of the *EML4-ALK* Transforming Gene in Non-Small Cell Lung Cancer

Young Lim Choi,¹ Kengo Takeuchi,³ Manabu Soda,^{1,2} Kentaro Inamura,³ Yuki Togashi,³ Satoko Hatano,³ Munehiro Enomoto,^{1,2} Toru Hamada,¹ Hidenori Haruta,¹ Hideki Watanabe,¹ Kentaro Kurashina,¹ Hisashi Hatanaka,¹ Toshihide Ueno,¹ Shuji Takada,¹ Yoshihiro Yamashita,¹ Yukihiko Sugiyama,² Yuichi Ishikawa,³ and Hiroyuki Mano^{1,4}

Divisions of ¹Functional Genomics and ²Pulmonary Medicine, Jichi Medical University, Tochigi, Japan; ³Department of Pathology, The Cancer Institute, Japanese Foundation for Cancer Research, Tokyo, Japan; and ⁴CREST, Japan Science and Technology Agency, Saitama, Japan

Abstract

The genome of a subset of non-small-cell lung cancers (NSCLC) harbors a small inversion within chromosome 2 that gives rise to a transforming fusion gene, *EML4-ALK*, which encodes an activated protein tyrosine kinase. Although breakpoints within *EML4* have been identified in introns 13 and 20, giving rise to variants 1 and 2, respectively, of *EML4-ALK*, it has remained unclear whether other isoforms of the fusion gene are present in NSCLC cells. We have now screened NSCLC specimens for other in-frame fusion cDNAs that contain both *EML4* and *ALK* sequences. Two slightly different fusion cDNAs in which exon 6 of *EML4* was joined to exon 20 of *ALK* were each identified in two individuals of the cohort. Whereas one cDNA contained only exons 1 to 6 of *EML4* (variant 3a), the other also contained an additional 33-bp sequence derived from intron 6 of *EML4* (variant 3b). The protein encoded by the latter cDNA thus contained an insertion of 11 amino acids between the *EML4* and *ALK* sequences of that encoded by the former. Both variants 3a and 3b of *EML4-ALK* exhibited marked transforming activity *in vitro* as well as oncogenic activity *in vivo*. A lung cancer cell line expressing endogenous variant 3 of *EML4-ALK* underwent cell death on exposure to a specific inhibitor of *ALK* catalytic activity. These data increase the frequency of *EML4-ALK*-positive NSCLC tumors and bolster the clinical relevance of this oncogenic kinase. [Cancer Res 2008;68(13):4971-6]

Introduction

Lung cancer is the leading cause of cancer deaths in the United States, with >160,000 individuals dying of this condition in 2006 (1). The efficacy of conventional chemotherapeutic regimens with regard to improving clinical outcome in lung cancer patients is limited. Activating mutations within the epidermal growth factor receptor gene (*EGFR*) have been identified in non-small-cell lung cancer (NSCLC), the major subtype of lung cancer (2, 3), and chemical inhibitors of the kinase activity of *EGFR* have been found to be effective in the treatment of a subset of NSCLC patients harboring such mutations. However, these somatic mutations of

EGFR are prevalent only among young women, nonsmokers, and Asian populations (3, 4).

We recently identified a novel transforming fusion gene, *EML4* (echinoderm microtubule-associated protein-like 4)-*ALK* (anaplastic lymphoma kinase), in a clinical specimen of lung adenocarcinoma from a 62-year-old male smoker (5). This fusion gene was formed as the result of a small inversion within the short arm of chromosome 2 that joined intron 13 of *EML4* to intron 19 of *ALK* (transcript ID ENST00000389048 in the Ensembl database⁵). The *EML4-ALK* protein thus contained the amino-terminal half of *EML4* and the intracellular catalytic domain of *ALK*. Replacement of the extracellular and transmembrane domains of *ALK* with this region of *EML4* results in constitutive dimerization of the kinase domain of *ALK* and a consequent increase in its catalytic activity (5).

Whereas this *EML4-ALK* fusion gene was detected in 3 of 75 individuals with NSCLC, we further identified another isoform of *EML4-ALK* in two patients of the same cohort (5). In these two individuals, intron 20 of *EML4* was disrupted and joined to intron 19 of *ALK*, with the fusion protein thus consisting of the amino-terminal two thirds of *EML4* and the intracellular domain of *ALK*. This larger version of *EML4-ALK* was referred to as variant 2, with the original smaller version being termed variant 1. A total of 5 of the 75 (6.7%) patients in the cohort were thus positive for *EML4-ALK*.

Given that detection of *EML4-ALK* cDNA by the PCR would be expected to provide a highly sensitive means for diagnosis of lung cancer, and given that inhibition of the catalytic activity of *EML4-ALK* may be an effective approach to treatment of this disorder, we have examined whether other isoforms of *EML4-ALK* are associated with NSCLC. We now describe a third isoform of *EML4-ALK* (variant 3) that is smaller than variants 1 and 2.

Materials and Methods

PCR. This study was approved by the ethics committees of Jichi Medical University and The Cancer Institute of the Japanese Foundation for Cancer Research. Total cDNA of NSCLC specimens was synthesized with PowerScript reverse transcriptase (Clontech) and an oligo(dT) primer from total RNA purified with the use of an RNeasy Mini RNA purification kit (Qiagen). Reverse transcription-PCR (RT-PCR) to amplify the fusion point of *EML4-ALK* variant 3 mRNA was done with a QuantiTect SYBR Green kit (Qiagen) and the primers 5'-TACCAGTGCTGTCTCAATTGCAGG-3' and 5'-TCTTGCCAGCAAAGCAGTAGTTGG-3'. A full-length cDNA for *EML4-ALK*

Note: Supplementary data for this article are available at Cancer Research Online (<http://cancerres.aacrjournals.org/>).

Requests for reprints: Hiroyuki Mano, Division of Functional Genomics, Jichi Medical University, 3311-1 Yakushiji, Shimotsukeshi, Tochigi 329-0498, Japan. Phone: 81-285-58-7449; Fax: 81-285-44-7322; E-mail: hmano@jichi.ac.jp.

©2008 American Association for Cancer Research.
doi:10.1158/0008-5472.CAN-07-6158

⁵ <http://www.ensembl.org/index.html>

variant 3 was amplified from total cDNA of a NSCLC specimen (ID no. 2075) with PrimeSTAR HS DNA polymerase (Takara Bio) and the primers 5'-ACTCTGTCCGGTCCGCTGAATGAAG-3' and 5'-CCACGGTCTTAGG-GATCCCAAGG-3'; PCR was done for 35 cycles of 98°C for 10 s and 68°C for 6 min. The fusion point of *EML4-ALK* in the genome was amplified by PCR with genomic DNA of NSCLC specimens, PrimeSTAR HS DNA polymerase, and the primers 5'-GGCATAAAGATGTCATCATCAAC-CAAGG-3' and 5'-AGCTTGCTCAGCTTGTACTCAGGG-3'. The nucleotide sequences of the *EML4-ALK* variant 3a and 3b cDNAs have been deposited in DDBJ/EMBL/GenBank under accession nos. AB374361 and AB374362, respectively.

Fluorescence in situ hybridization. Fluorescence *in situ* hybridization (FISH) analysis of the fusion gene was done with archival pathology specimens and with bacterial artificial chromosomes containing genomic DNA corresponding to *EML4* or *ALK* and their flanking regions as probes. In brief, surgically removed lung cancer tissue was fixed in 20% neutral

buffered formalin, embedded in paraffin, and sectioned at a thickness of 3 μm. The sections were placed on glass slides and processed with a Histology FISH Accessory Kit (DakoCytomation) before hybridization with the *EML4* and *ALK* probes and examination with a fluorescence microscope (BX61, Olympus).

Transforming activity of *EML4-ALK* variant 3. Analyses of the function of *EML4-ALK* variant 3 were done as described previously (5). In brief, the cDNA for *EML4-ALK* variant 3a or 3b was fused with an oligonucleotide encoding the FLAG epitope tag and then inserted into the retroviral expression plasmid pMXS (6). The resulting plasmids as well as similar pMXS-based expression plasmids for *EML4-ALK* variant 1, variant 1 (K589M), or variant 2 were individually introduced into mouse 3T3 fibroblasts by the calcium phosphate method for a focus formation assay and assay of tumorigenicity in nu/nu mice. The same set of *EML4-ALK* proteins was expressed in HEK293 cells and assayed for kinase activity *in vitro* with the YFF peptide (7).

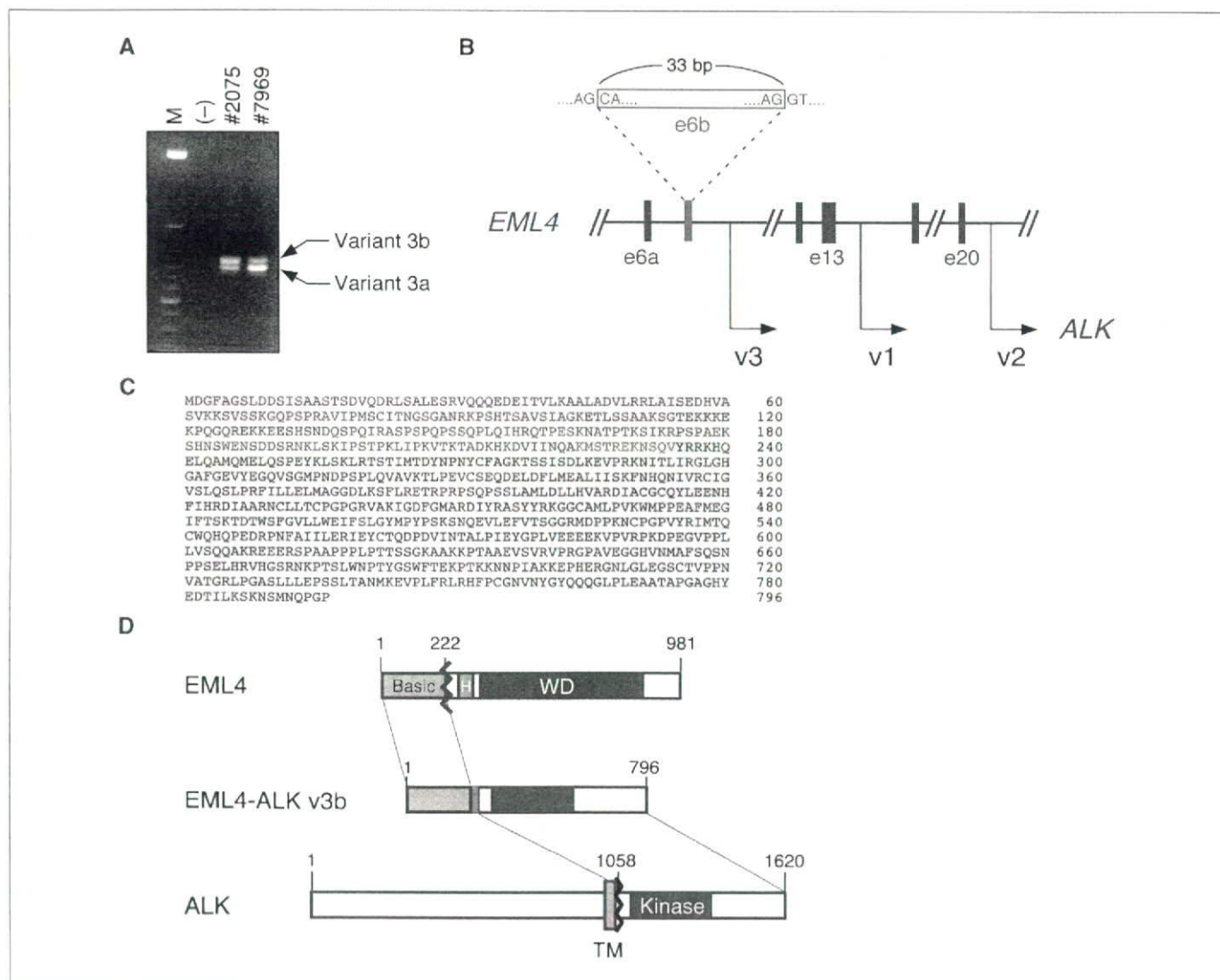


Figure 1. Identification of *EML4-ALK* variant 3. **A**, detection of fusion cDNAs linking exon 6 of *EML4* to exon 20 of *ALK* by RT-PCR analysis. Two RT-PCR products of 548 bp (corresponding to variant 3b) and 515 bp (corresponding to variant 3a) were detected by agarose gel electrophoresis with total RNA from two NSCLC specimens (tumor ID nos. 2075 and 7969). Lane (-), no-template control; lane M, size markers (50-bp ladder). **B**, genomic organization of *EML4*. Intronic sequences downstream of exons (e) 6, 13, and 20 of *EML4* are fused to intron 19 of *ALK* to generate variants (v) 3, 1, and 2 of *EML4-ALK*, respectively. Exon-intron boundary sequences as well as the size of exon 6b are indicated. **C**, predicted amino acid sequence of *EML4-ALK* variant 3b. Blue, green, and red, amino acids corresponding to exons 1 to 6a of *EML4*, exon 6b of *EML4*, and *ALK*, respectively. Amino acid number is indicated on the right. **D**, fusion of an amino-terminal portion of *EML4* [which consists of a basic region (Basic), HELP domain (H), and WD repeats] to the intracellular region of *ALK* (containing the tyrosine kinase domain) generates *EML4-ALK* variant 3b. Green, the region of the fusion protein encoded by exon 6b of *EML4*. TM, transmembrane domain.